



Theses and Dissertations

2019-12-10

Controller Design for Coordinated Encirclement of Moving Targets

Puneet Jain
Brigham Young University

Follow this and additional works at: <https://scholarsarchive.byu.edu/etd>



Part of the [Physical Sciences and Mathematics Commons](#)

BYU ScholarsArchive Citation

Jain, Puneet, "Controller Design for Coordinated Encirclement of Moving Targets" (2019). *Theses and Dissertations*. 8712.

<https://scholarsarchive.byu.edu/etd/8712>

This Thesis is brought to you for free and open access by BYU ScholarsArchive. It has been accepted for inclusion in Theses and Dissertations by an authorized administrator of BYU ScholarsArchive. For more information, please contact ellen_amatangelo@byu.edu.

Controller Design for Coordinated Encirclement of Moving Targets

Puneet Jain

A thesis submitted to the faculty of
Brigham Young University
in partial fulfillment of the requirements for the degree of
Master of Science

Cameron K Peterson, Chair
Randal W Beard
Marc D Killpack

Department of Electrical and Computer Engineering
Brigham Young University

Copyright © 2019 Puneet Jain

All Rights Reserved

ABSTRACT

Controller Design for Coordinated Encirclement of Moving Targets

Puneet Jain

Department of Electrical and Computer Engineering, BYU

Master of Science

This thesis presents controllers that use relative range and bearing measurements to steer unmanned aerial vehicles (UAVs) to circular trajectories around stationary, constantly moving and constantly accelerating targets. The range and bearing to the target, along with their derivatives are estimated. These, along with the estimated local heading of the UAVs, are used in the control law, and to estimate the velocity of the target. In this work, six controllers are presented. The controller for a stationary target is derived using Lyapunov's direct method, and feedback linearization is used for the constant velocity and accelerating targets. A new controller is proposed to control the direction of encirclement for moving targets, using Lyapunov's direct method. Additional terms are introduced to maintain a temporally equi-spaced formation around the targets. Theoretical proofs are provided for all controllers using Lyapunov theory.

Numerical simulations show vehicles converging to circular formations around both stationary and moving targets. Results are shown using MATLAB simulations with Gaussian noise added to the measurements. Further, a technique is proposed for information exchange between UAVs, with bounds provided for the time taken to dissipate information throughout the system in a scenario with multiple groups of UAVs tracking multiple targets.

Keywords: encirclement, stability, simulations, feedback linearization

ACKNOWLEDGMENTS

Firstly, I want to thank Dr. Cammy Peterson, for her support from the beginning of my Masters program. This thesis has been majorly built up on the work done by her during her PhD, and through her inputs and support I was able to contribute and learn all the things I did through this journey and put this thesis together. Her invaluable contributions throughout my Masters, in terms of knowledge, guidance and support have helped me write this thesis.

I would then like to thank my family members, (in alphabetical order) - Mr. Ajay Jain, Mr. Akshay Jain, Ms. Kanika Choudhary, Mr. Mahendra Kumar Jain, Ms. Maitri Jain, Mr. Sanjay Jain, Mrs. Santosh Jain, Mr. Shashank Jain, Mrs. Suman Jain, and Mrs. Sushma Jain. Their support – emotional and spiritual, throughout the journey made me endure it. Their belief that I could work through, living away from home for the first time and learning to live on my own was monumental in the decisions I made throughout my research work.

I would also like to thank my committee members Dr. Randal Beard and Dr. Mark Killpack who gave me valuable inputs and were willing to help throughout the journey.

I would also like to thank all the administrative staff (Kris, Mark, and all the international office!) for all their support and answering my un-ending questions about being an international student and other problems that I faced throughout my graduate degree.

Lastly, and most importantly, I thank the eternal power, who sent everyone else in my life, my friends, who fed me, reviewed my thesis, and motivated me; my roommates who made me feel at home across the world; my colleagues and classmates that helped me at every turn in adapting to BYU; and my doctors (and my sister who is almost a doctor), who helped me fight through the health issues I faced moving to Utah. With their constant support and teachings throughout the journey, I was able to complete this thesis.

TABLE OF CONTENTS

TABLE OF CONTENTS	iv
List of Figures	vi
Nomenclature	viii
Chapter 1 Introduction	1
1.1 Motivation	1
1.2 Contribution	3
Chapter 2 Dynamic Models of UAV and Target	7
2.1 UAV Model	7
2.2 Target Model	8
Chapter 3 Controller Design	10
3.1 Lyapunov Based Control for Stationary Targets	12
3.2 Encirclement of Constant Velocity Targets	13
3.3 Direction Control While Encircling Constant Velocity Targets	19
3.4 Encirclement of Constantly Accelerating Targets	22
3.5 Direction Control While Encircling Constant Acceleration Targets	24
Chapter 4 Multi-Agent Coordination	26
4.1 Time-Splay Formations	26
4.2 Gossip Algorithms for Inter-Group Communication	31
Chapter 5 Encirclement Using only Relative Measurements: Noise Considerations and Estimation	36
5.1 Noise Considerations	36
5.2 Estimation for Constant Velocity Targets	37
Chapter 6 Simulations and Results	41
6.1 Stationary Targets	41
6.2 Constant Velocity Moving Targets	43
6.3 Directional Control with Constant Velocity Targets	44
6.4 Consistency of the Filter and Target Velocity Estimates for Constant Velocity Targets	45
6.5 Constantly Accelerating Targets	46
6.6 Constantly Accelerating Targets with Direction Control	47
Chapter 7 Conclusion	50
7.1 Control Strategies	50
7.2 Multi-Agent Coordination	51

REFERENCES	53
Appendix A Stationary Target Encirclement with Speed Control	58

LIST OF FIGURES

2.1	The axes represent the local frame of UAV _k . All definitions are in this local frame. The current heading of the target at position p_k is ψ_k and its velocity is $v_{x_k} + iv_{y_k}$	8
3.1	Instantaneous circle center of UAV moving at speed one and for radius ω_0^{-1}	11
3.2	UAV encirclement of a stationary target with a desired radius of 30m.	14
3.3	Figure that depicts transient cases where the matrix $G(q)$ is not full rank. This happens when one component, the X or the Y, of the velocity of the UAV and target are equal, and $\alpha + \theta = \pm \frac{\pi}{2}$. Here, the X component is equal and the UAV is directly below the target, with $\alpha + \theta = \frac{\pi}{2}$. This degenerate case could also occur if $\dot{r}_y = v_y$	16
3.4	Constant velocity target encirclement. Velocity of the target is $v_x + iv_y = 0.4 - i0.1m/s$	19
3.5	Target encirclement in clockwise direction for target moving with velocity $v_x = 0.4m/s$	21
3.6	Encirclement of a constantly accelerating target with $a_x + ia_y = (-0.0001 + i0.0001)m/s^2$ and initial velocity $v_x + iv_y = (0.4 - i0.1)m/s$	23
3.7	Target encirclement in clockwise direction for target moving with initial velocity $v_x + iv_y = (0.4 - i0.1)m/s$ and acceleration $a_x + ia_y = (-0.0001 + i0.0001)m/s^2$	25
4.1	Different symmetric formations for a four UAV scenario in a stationary target case: (left) Coordinated, (middle) Two-tuple, (right) Symmetric. See also [1].	27
4.2	(left) Seven UAVs in the inertial frame in a time-splay formation around a constant velocity target moving with velocity $v_x + iv_y = (0.4) m/s$ and (right) the local angle γ_k of the UAV evolving from random positions to a time-splay formation.	32
4.3	Mobility process linking five groups of UAVs with an example three UAVs in every group, μ_i is the probability at every time step for a UAV to leave group i . Denoted is an example with UAV leaving Group 1. $\rho = \frac{1}{n-1} = \frac{1}{4}$ is the probability that a person who leaves region i travels to region j , which is evenly distributed for all other four groups.	33
4.4	Time for information dissipation decreases with increasing probability of movement between groups. The x-axis denotes the probability of movement of UAVs between groups, and y-axis shows the time-to-spread the information, which is averaged over 100 simulation runs.	35
6.1	Trajectory of UAV encircling a stationary target for simulation time $t = [0,10000]s$	42
6.2	Bearing α_k (left) and range β_k (right) of the target with respect to the UAVs as a function of time for a stationary target.	42
6.3	Trajectory of UAVs encircling a target moving with constant velocity $v_x + iv_y = (0.4 - i0.1)m/s$ for simulation time $t = [1,1000]s$ in the inertial frame (left) and target moving frame (right).	43
6.4	Bearing α_k (left) and range β_k (right) to the target with respect to the UAV as a function of time for a moving target with velocity $v_x + iv_y = (0.4 - i0.1)m/s$	44
6.5	Constant velocity target encirclement with direction control in an inertial (left) and target moving frame (right) with velocity $v_x + iv_y = (0.4 - i0.1)m/s$	45
6.6	Bearing (left) and range (right) from target for a constant velocity target encirclement with direction control with velocity $v_x + iv_y = (0.4 - i0.1)m/s$	45

6.7	Consistency test for bearing (left) and range (right) for a random UAV. The red solid line shows the real bearing α_k . The shaded region shows the 2σ covariance bounds from the estimate shown with the blue solid line. The left figure shows the first 20s window to better see the real α_k enclosed by the bounds.	46
6.8	Estimated velocities (left: \hat{v}_x , right: \hat{v}_y) in an inertial frame, for a constant velocity target. The estimates have about 10 times the noise levels of the magnitude of the actual target velocities. The dashed blue line is the true value of the velocities in the inertial frame.	47
6.9	Constantly accelerating target encirclement in an inertial (left) and target moving frame (right) with initial velocity $v_x + iv_y = (0.4 - i0.1)m/s$ and acceleration $a_x + ia_y = (-0.0001 + i0.0001)m/s^2$	47
6.10	Bearing (left) and range (right) from a constantly accelerating target with initial velocity $v_x + iv_y = (0.4 - i0.1)m/s$ and acceleration $a_x + ia_y = (-0.0001 + i0.0001)m/s^2$	48
6.11	Constantly accelerating target encirclement with direction control in an inertial (left) and target moving frame (right) with initial velocity $v_x + iv_y = (0.4 - i0.1)m/s$ and acceleration $a_x + ia_y = (-0.0001 + i0.0001)m/s^2$	48
6.12	Bearing (left) and range (right) from a constantly accelerating target with direction control. The initial velocity is $v_x + iv_y = (0.4 - i0.1)m/s$ and acceleration is $a_x + ia_y = (-0.0001 + i0.0001)m/s^2$	49
7.1	Communication setup for an example two UAVs	52
A.1	(left) The UAV converges to the loiter circle. (right) The range converges to 30m.	59

NOMENCLATURE

N	number of UAVs
X_k	X-axis of the k th UAV
Y_k	Y-axis of the k th UAV
θ_k	Local heading angle of the k th UAV in it's reference frame
α_k	Bearing of the target from the k th UAV
β_k	Range of target from the k th UAV
p_k	position of the target in the frame of k th UAV
r_k	position of the k th UAV in it's local frame
s	Speed of the UAVs
v	Speed of the target
v_{x_k}	X-velocity of the target in the frame of k th UAV
v_{y_k}	Y-velocity of the target in the frame of k th UAV
ψ_k	Angle of the travel of target in the frame of k th UAV
ω_0	Desired angular speed of the UAVs
u_k	Control input for a given controller for the k th UAV
$\alpha_{k,d}$	Desired bearing of the target for the k th UAV
d	Variable to control the direction of encirclement
v_i	probability of a UAV leaving a group i to travel to another group

CHAPTER 1. INTRODUCTION

With the increasing demand of UAVs for various tasks such as tracking, surveillance, delivery, defense, photography, and even entertainment, research is being done to make the UAVs better at executing these tasks. In this thesis, we focus on a limited use case; encirclement of a target using estimated relative measurements. In this chapter, we will motivate the work done in this thesis, discussing earlier work done in the domain of target encirclement and summarize our contributions in the field.

1.1 Motivation

Encirclement using UAVs is applicable to tasks like the tracking and surveillance of protected areas such as those used to prevent illegal poaching or fishing. UAVs provide a great platform for surveillance and detection of these activities without posing a risk to researchers or animals, and with minimal disturbance to the environment [2]. Encirclement using relative measurements can also be applicable to fly over military vehicles in the warfield, encircling a scout or group, and giving them situational awareness of an area [3]. This method can also be used to make a UAV follow a hiker on a trail through the grasslands, recording adventures and making it easier for search and rescue missions in case of mishaps [4].

Keeping the target in the field of view of a sensor, like a camera or radar, is an essential element of target tracking [5]. Doing so improves the predictions of where the target is with respect to the UAV. Target encirclement helps to achieve this goal by keeping the target in the center of a fixed radius trajectory, and thus giving the UAV time to adjust to the target's estimated motion.

In GPS-denied environments, target encirclement can be achieved using range and bearing measurements from sensors like radar and LIDAR [6], [7]. A camera is commonly used with UAVs for target identification and tracking in GPS-denied environments [8], since it is cost-effective, lightweight, and less energy consuming. It can also be adapted with IMU measurements to get

bearing and an estimated range from the target. We can get the range using depth estimation approaches for monocular cameras [9–12], stereo cameras [13], combined camera and laser range finders [14–16] and using radars with cameras [17]. This thesis provides an approach to track and encircle moving targets in a way that applies to UAVs carrying only cameras, focusing only on the control aspect of the problem.

Target encirclement is a widely discussed topic in the literature. Zhang et al. [18] proposed an encirclement approach for moving targets based on sliding mode control, but they assumed a common inertial frame for tracking. Frew et al. [19] used Lyapunov guidance vector fields and proved stable convergence to a circular trajectory around a stationary target. They also assumed that the vehicle knew its position in a local inertial frame relative to the target. In [20], [21], range and range-rate based controllers were proposed for encircling stationary targets. Matveev et al. [22] proposed a sliding mode controller based on range and range-rate for a circumnavigating using a ground robot with a Dubins model. They further provided proof of convergence for a stationary target but their controller lacks global convergence. In [23], target tracking was presented using bearing-only measurements from the target. Their method stabilized circular formations for stationary targets and mildly perturbed targets. These works on target encirclement assume perfect knowledge of the target and the UAV's inertial position or the distances and angles between them in a common local frame.

Research that proposes controllers for noisy sensor data includes [24–26]. In [24], Hashemi et al. discussed additive sensor noise but did not propose an estimator. They showed that their controller for stationary targets could achieve a constant radius circle with the noise. The Lyapunov vector field approach is further explored by Summers et al. [25]. In this work, the authors proposed a variable airspeed controller to stabilize circular motion for constant velocity targets with estimated measurements of range and bearing. Oh et al. [26] also discussed the vector field guidance approach and focused on tangential vector fields with estimation of target motion. They proposed using a ground moving target indicator (GMTI) sensor with a decentralized extended information filter for updating the UAV states and sharing them with other UAVs. For multiple vehicles, they assumed knowledge of a common local frame.

Other related work in target encirclement includes: [27], which discussed different approaches to target encirclement like a Helmsman behaviour and Lyapunov vector field based guid-

ance laws, controlled collective behaviour, and real-time optimized model predictive control. They compare results using simulations with noise added to the system. In [28], a camera is used to guide a UAV to a given target viewing angle and then spiral around the target with a changing radius. They focus on a stationary target and maintaining a given camera angle for the sensing aspect of tracking while changing the radius for maintaining the best field of view.

Most of the earlier works either do not talk about maneuvering targets or use perfect knowledge of the target. Many of them also assume knowledge of a common frame of reference for tracking and communication.

1.2 Contribution

The work in this thesis takes inspiration from [22], [25] and [29] who all provide encirclement of targets moving with constant velocity. However, in this work, the control algorithms are framed assuming no information of the UAV positions in a global or local inertial frame common to all UAVs. The UAV has knowledge of its heading change at every time step, which is commanded by our controller, to estimate the heading in a local frame. For better readability and ease of understanding, we also assume that all the UAVs move with a constant, unit speed. This velocity represents either the UAV's maximum speed or its most energy efficient speed. This assumption does not change the dynamics, and the work is applicable to UAVs moving with any constant speed. Stability of the controllers to drive the UAVs to a constant radius circle around the target is proven. Figure 2.1 describes the scenario we use in this thesis, with k UAVs having their own frame. Each UAV gets bearing and range measurements from the target.

For stationary targets, we design a controller which uses only the estimated values of range and bearing to the target, to steer the UAVs. Even knowledge of the local inertial frame is not needed for stationary target encirclement. This work is extended to targets moving with constant velocity using a feedback linearization control law. In this case, the relative range, bearing, and UAV's change in heading are used to compute the control law. We estimate both the target motion and relative UAV-target measurements and use those estimates in the control algorithms. Results are provided for encircling targets with estimated motion using noisy measurements of range and bearing.

This proposed controller, although it makes the UAVs converge to loiter circles, does not give us control over the direction of encirclement. Earlier works do not explicitly talk about direction of encirclement, except [29]. Some works ([25], [30]) show only one direction of encirclement. This is not explicitly stated, but might be due to the initial conditions, or their proposed controller converging the vehicles in a single direction only. Control over the direction is important for real applications to avoid collisions and help us maintain certain formations, like equi-spaced or equi-temporally spaced UAVs around a circle, as we will discuss in Section 4.1. We show results for a controller which is able to specify the direction of encirclement while encircling constant velocity targets.

We further propose a controller which encircles targets moving with constant acceleration using feedback linearization, and one using Lyapunov's direct method to control the direction of encirclement. Simulation results for the accelerating targets with noisy measurements but known acceleration are provided. As far as we know, target encirclement for accelerating targets has not been explored in a relative framework, except a locally stable controller in [22] and a controller based on a stochastic approach with no stability proofs or guarantees of convergence to a desired radius [31].

Even though in our work, each UAV has its own frame of reference, we extend the work from [29], [32] to arrange the UAVs in a constant-time-separation (time-splay) formation for efficient coverage on the circle using the estimated local heading of each UAV and their estimate of the target velocity. A rotationally symmetric potential function dependant on the relative heading in the moving target frame is used to maintain the splay formation. This enables the UAV formations to robustly re-arrange themselves in cases of UAV injection or attrition, while still encircling targets.

We further propose a solution for applications such as tracking and search in large areas like forests and oceans. In these scenarios, UAVs are much farther from each other than their communication range, and do not have a central network. Thus, it is difficult to communicate the status of the tasks between the UAV groups. Reliable communication and information spread between multiple groups of UAVs can help us complete the given task efficiently.

Inspired from the model of the spread of epidemics in [33], and gossip algorithms, which are widely used in relaying information and optimization for homogenous autonomous groups [34],

[35], we use a probabilistic inter-group movement model for inducing travel of UAVs between different groups. A UAV that is sharing information by travelling between groups is called a messenger UAV. UAVs are assumed to have a fixed, circular radio communication range which enables them to share the latest information they have about all the other UAVs. We present results of information dispersion times throughout the system for the stationary target case when varying the frequency of inter-group UAV travel, assuming the travellers know the position of the current groups. Future work will include incorporating the relative-measurement and estimation framework into inter-group travel.

The specific contributions of this thesis include:

- An asymptotically stable controller to drive UAVs to encircle a *stationary* target using only range and bearing measurements from the target.
- Two theoretically stable control algorithms to encircle a *constant velocity* target (one with direction control, one without) using the UAV's change in heading and relative UAV-target measurements.
- Two theoretically stable control algorithms to encircle a *constantly accelerating* target (one with direction control, one without) using the UAV's change in heading and relative UAV-target measurements.
- An estimator to approximate variables used in the control algorithms for constant velocity and stationary target cases including relative measurements of range and bearing, the local heading, and the target velocity.
- A controller to encircle constant velocity targets in a time-splay formation without global knowledge of other UAVs.
- A bound on the time-to-spread information in the scenario of multiple groups of UAVs using messenger vehicles to communicate between groups.

This thesis proceeds as follows. In Chapter 2, we describe the UAV and target models. Chapter 3 proposes controllers for stationary, constant velocity and constantly accelerating targets,

and gives proofs of their convergence to encircle a target. The multi-UAV time-splay and multi-group information spread time bounds are presented in Chapter 4. We present the sensor noise considerations and an estimation framework in Chapter 5. In Chapter 6, we present results from numerical simulations for our proposed controllers and estimator. Conclusions and future work are given in Chapter 7.

CHAPTER 2. DYNAMIC MODELS OF UAV AND TARGET

In this chapter, the models and assumptions for both the UAV (Section 2.1) and the target (Section 2.2) are described. We use a unicycle model to represent the dynamics of the UAV, and different models: stationary, constant velocity and constant acceleration, for the target.

2.1 UAV Model

This work uses a unicycle model in a two dimensional plane to represent the UAV motion. This type of model has been used frequently in the literature [36–38]. In this model, the UAV is able to control its turn-rate and travels at a constant unit speed. The constant speed represents a constant airspeed UAV, and thus there is no control effort to regulate the speed, but only the lateral motion. The dynamics in the complex plane for the k th UAV at position r_k are

$$\begin{aligned}\dot{r}_k &= e^{i\theta_k} = \cos(\theta_k) + i \sin(\theta_k) \\ \dot{\theta}_k &= u_k,\end{aligned}\tag{2.1}$$

where i is the unit imaginary number, \dot{r}_k is the velocity and θ_k is the heading of UAV $_k$ in its local frame. Note the implied one in front of the exponent of the velocity following our assumption that all the UAVs travelling at unit speed. In a multi-UAV scenario, the local frame of reference for each UAV is set arbitrarily using the UAV's initial heading. Figure 2.1 shows the local frame where X_k is aligned with the UAV $_k$'s initial heading. The range and bearing to the target are β_k and α_k , respectively. The heading of the target is ψ_k in the k th UAV's local frame. In this frame the target has a velocity $v_{x_k} + iv_{y_k}$. The input control u_k is used to change the UAV $_k$'s heading.

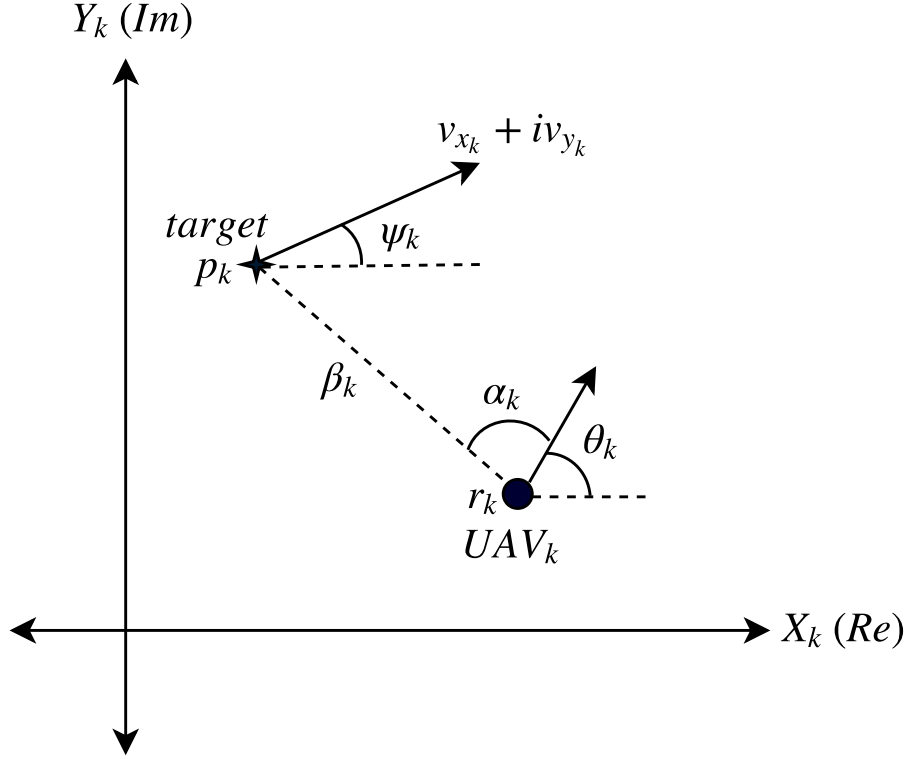


Figure 2.1: The axes represent the local frame of UAV_k . All definitions are in this local frame. The current heading of the target at position p_k is ψ_k and its velocity is $v_{x_k} + i v_{y_k}$.

Additionally, we place a turn-rate constraint on each UAV to mimic its bank angle limit, by saturating the control with u_{max} .

$$u_k = \begin{cases} -u_{max}, & u_k < -u_{max} \\ u_k, & -u_{max} \leq u_k \leq u_{max} \\ u_{max}, & u_k > u_{max} \end{cases} . \quad (2.2)$$

2.2 Target Model

The heading of the target in the k th UAV's local frame is ψ_k . In this frame the target has position p_k . The position of the target is the desired center of the circle. We use three different models for target motion: 1. stationary targets, 2. constant velocity targets, and 3. constant

acceleration targets. The target acceleration is defined as

$$\ddot{p}_k = a_{x_k} + ia_{y_k},$$

and the target velocity is defined as

$$\dot{p}_k = v_{x_k} + iv_{y_k}.$$

In the case of stationary targets $a_{x_k} = a_{y_k} = v_{x_k} = v_{y_k} = 0$. For constant velocity targets, v_{x_k} and v_{y_k} are constants. In case of accelerating targets, a_{x_k} and a_{y_k} are constants and velocities and positions of the target are calculated using

$$v_k = v_k^- + a_k \Delta t$$

$$p_k = v_k^- \Delta t + \frac{(\Delta t)^2}{2} a_k,$$

where v_k^- is the initial velocity, and $\Delta t = t - t_0$, where t_0 is the starting time.

For this thesis, we assume that the speed of the target $v_k = \sqrt{v_{x_k}^2 + v_{y_k}^2}$ is always less than the speed of the UAVs (unit speed), even in the case of accelerating targets $v_k < 1$. We enforce this in the simulations by always keeping the acceleration low enough that the speed doesn't go above one in the given simulation time.

CHAPTER 3. CONTROLLER DESIGN

In this chapter, we propose provably stable controllers for encirclement of stationary, constant velocity, and constantly accelerating targets. For stationary targets, the controller uses only range and bearing from the target to encircle it. For moving targets, the controllers use the range and bearing from the target, along with the UAVs local heading to encircle the moving target. We also propose controllers to incorporate a desired direction of encirclement for moving targets. The controllers assume that the UAVs travel at unit speed for the ease of understanding and simplicity of the equations. A controller with a non-unit speed UAV that encircles a stationary target is described in Appendix A. Also in this chapter, because the control algorithms operate on each UAV individually, the subscript k for the UAV index is removed, and the control behavior is demonstrated for a single UAV.

The instantaneous circle center for the UAV is [29]

$$c = r + d\omega_0^{-1}ie^{i\theta}, \quad (3.1)$$

where $\omega_0 > 0$ is the angular speed of the UAV and the direction of encirclement is governed by $d = \pm 1$ ($d = -1$ indicates a clockwise direction and $d = 1$ a counter-clockwise direction). Figure 3.1 depicts the current center of the UAV traveling in a clockwise direction. Since the UAV has unit speed, ω_0^{-1} is the circle's radius. The parameter ω_0^{-1} is used to set the radius of the loiter circle. The desired center of the circle is the target position, which is denoted by p in the inertial frame. The target is at a distance β and at an azimuth angle α from the UAV. This is denoted by

$$p = r + \beta e^{i(\theta+\alpha)},$$

where α and β are

$$\alpha = \tan^{-1}\left(\frac{p_y - r_y}{p_x - r_x}\right) - \theta \quad (3.2)$$

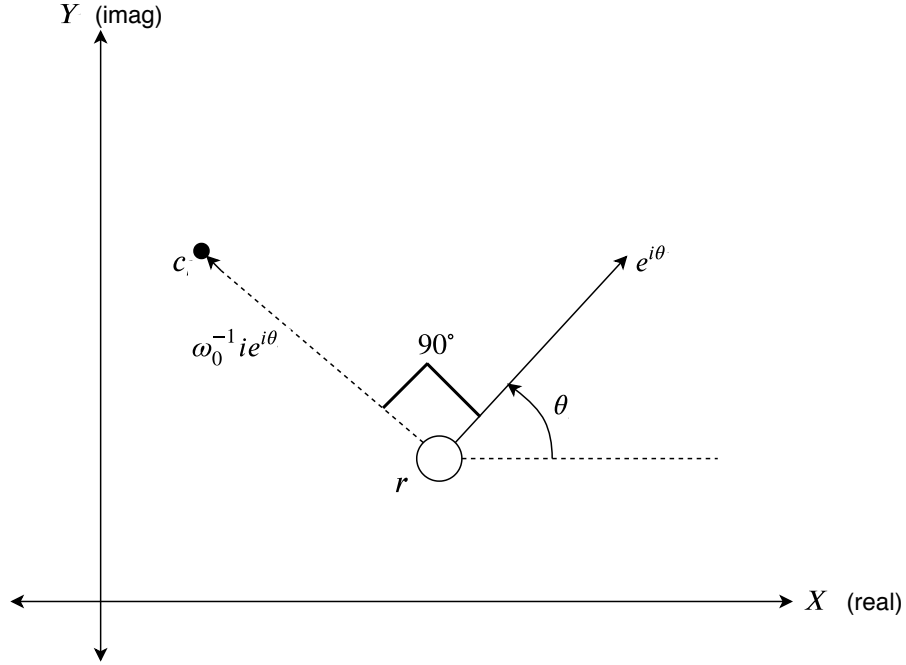


Figure 3.1: Instantaneous circle center of UAV moving at speed one and for radius ω_0^{-1} .

and

$$\beta = \sqrt{(p-r)^H(p-r)} = \|p-r\|_2. \quad (3.3)$$

The complex conjugate transpose (or Hermitian) is denoted by $[\cdot]^H$, and $\|\cdot\|_2$ is the Euclidean 2-norm. The real and imaginary part of the desired circle center (target position) are p_x and p_y and the UAV's X and Y positions are r_x and r_y .

Choosing the error $e = p - c$ to be the difference between the desired circle center and the actual circle center gives

$$e = p - c = \beta e^{i(\theta+\alpha)} - d\omega_0^{-1} i e^{i\theta}, \quad (3.4)$$

with error dynamics given by taking the derivative with respect to time,

$$\begin{aligned} \dot{e} &= \dot{p} - \dot{c} \\ &= \dot{\beta} e^{i(\alpha+\theta)} + i\beta e^{i(\alpha+\theta)} (\dot{\alpha} + \dot{\theta}) + d\omega_0^{-1} e^{i\theta} \dot{\theta}. \end{aligned} \quad (3.5)$$

The time derivatives of bearing and range from Equations (3.2) and (3.3) are

$$\dot{\alpha} = \frac{(p_x - r_x)(v_y - \dot{r}_y) - (p_y - r_y)(v_x - \dot{r}_x)}{(p_x - r_x)^2 + (p_y - r_y)^2} - u, \quad (3.6)$$

and

$$\dot{\beta} = \frac{(p_x - r_x)(v_x - \dot{r}_x) + (p_y - r_y)(v_y - \dot{r}_y)}{\sqrt{(p_x - r_x)^2 + (p_y - r_y)^2}}. \quad (3.7)$$

The geometric relationships between the target and UAV measurements as described in Figure 2.1 are

$$p_x - r_x = \beta \cos(\alpha + \theta) \quad (3.8)$$

$$p_y - r_y = \beta \sin(\alpha + \theta),$$

and

$$\dot{r}_x = \cos(\theta) \quad (3.9)$$

$$\dot{r}_y = \sin(\theta).$$

Substituting Equations (3.8) and (3.9) into Equations (3.6) and (3.7) for $\dot{\alpha}$ and $\dot{\beta}$ yields

$$\dot{\alpha} = \beta^{-1}(v_y \cos(\alpha + \theta) - v_x \sin(\alpha + \theta) + \sin(\alpha)) - u, \quad (3.10)$$

$$\dot{\beta} = v_x \cos(\alpha + \theta) + v_y \sin(\alpha + \theta) - \cos(\alpha). \quad (3.11)$$

These equations for the heading α and range β do not have any inertial frame information.

3.1 Lyapunov Based Control for Stationary Targets

In this section, we use a Lyapunov-based controller to show global asymptotic convergence of a UAV to a circle of fixed radius around the stationary target using relative sensor measurements.

Theorem 1. *All trajectories of a UAV following the dynamics of Equations (2.1) and using control law*

$$u = d\omega_0(1 - \beta \cos(\alpha)) \quad (3.12)$$

will globally asymptotically converge to a circle centered at a stationary target ($v_x = v_y = 0$) with radius ω_0^{-1} .

Proof. Consider the Lyapunov function $V = \frac{1}{2}e^H e$ whose derivative with respect to time is $\dot{V} = \text{real}(e^H \dot{e})$.

Let $S = \{(e, 0), (0, \dot{e}), (0, 0)\}$ be the set where $\dot{V}(e, \dot{e}) = 0$ and $E \subset S$ be the largest invariant set in S . We will show that $E = \{(0, 0)\}$ and in this set a UAV will encircle the stationary target.

Solving Equation (3.5) for $\dot{e} = 0$ provides two cases: $\beta = 0$ or $\cos(\alpha) = 0$. The first case, $\beta = 0$, is not part of the invariant set; the UAV travels at unit speed and cannot stay indefinitely over the stationary target.

In the second case, when $\cos(\alpha) = 0$, the range-rate is $\dot{\beta} = 0$, and thus β is constant. The controller (Equation (3.12)) is constant, $u = d\omega_0$, and the bearing-rate $\dot{\alpha} = \beta^{-1} - d\omega_0$ is also a constant and must equal zero since $\cos(\alpha) \equiv 0$. This implies that the range is $\beta = d\omega_0^{-1}$.

Furthermore, with values $\beta = d\omega_0^{-1}$ and $\alpha = \pm\pi/2$, $e = 0$ (Equation (3.4)). Thus, under the conditions when $\dot{e} = 0$ is invariant, then $e = 0$. It can similarly be shown that the invariant case for $e = 0$ yields the same conditions on α and β and requires that $\dot{e} = 0$. Therefore, $E = \{(0, 0)\}$ is the largest invariant set.

According to the Lasalle's invariance theorem ([39], Theorem 4.4, Corollary 4.1), the system will asymptotically converge to E where $\beta = \omega_0^{-1}$ and $\alpha = \pm\pi/2$ with the sign determined by the sign of d . These are the conditions required for a UAV following dynamics from Equation (2.1) to encircle a stationary target with radius ω_0^{-1} and the direction determined by d .

□

Figure 3.2 shows convergence of a UAV to a 30m radius circle around a stationary target. The blue “+” shows the target, the pink “+” shows the initial position of the UAV, and the dashed line shows the trajectory of the UAV.

Note that the control (Equation (3.25)) is only a function of the relative measurements α and β , therefore no inertial or even local UAV frame information is needed to command the UAV to encircle the target.

3.2 Encirclement of Constant Velocity Targets

In this section, we present a feedback linearization approach to find an exponentially stable controller to encircle moving targets. We consider a constant velocity target where $\dot{p} \neq 0$. The

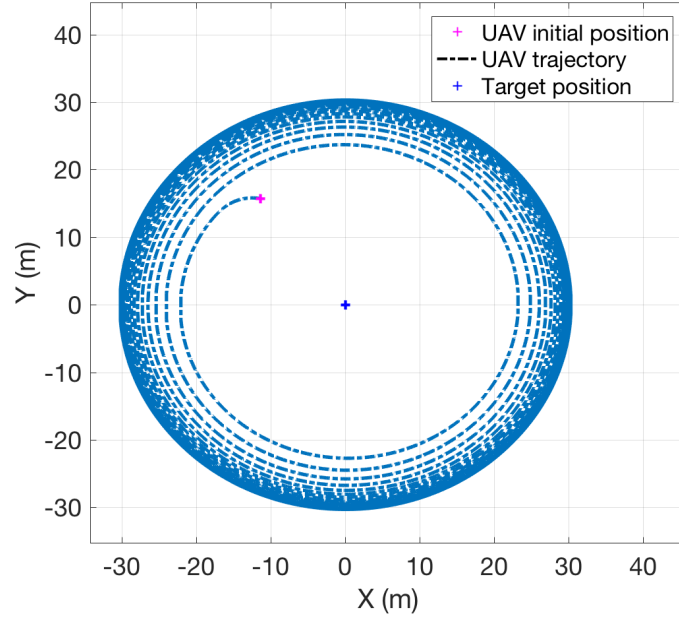


Figure 3.2: UAV encirclement of a stationary target with a desired radius of 30m.

error dynamics are defined as in Equation (3.5). For the purpose of encircling moving targets, we start by defining the state vector for each UAV as

$$q = \begin{bmatrix} q_1 \\ q_2 \end{bmatrix} = \begin{bmatrix} \alpha \\ \beta - \omega_0^{-1} \end{bmatrix}. \quad (3.13)$$

From Equations (3.10) and (3.11)

$$\begin{aligned} \dot{q} &= \begin{bmatrix} \dot{\alpha} \\ \dot{\beta} \end{bmatrix} \\ &= \underbrace{\begin{bmatrix} \beta^{-1}(v_y \cos(\alpha + \theta) - v_x \sin(\alpha + \theta) + \sin(\alpha)) \\ v_x \cos(\alpha + \theta) + v_y \sin(\alpha + \theta) - \cos(\alpha) \end{bmatrix}}_{f(q)} \\ &\quad + \underbrace{\begin{bmatrix} -1 \\ 0 \end{bmatrix}}_{g(q)} u. \end{aligned} \quad (3.14)$$

The system $\dot{q} = f(q) + g(q)u$ is feedback linearized assuming known constant velocities v_x and v_y of the target. In Chapter 5 this assumption will be removed using a method to estimate them.

The system is feedback linearizable if the following holds ([39], Theorem 13.2): 1. $\Delta = \text{span}\{g(q), ad_f g(q), \dots, ad_f^{m-2} g(q)\}$ is involutive and 2. $G(q) = [g(q), ad_f g(q), \dots, ad_f^{m-1} g(q)]$ has rank m , where m is the number of states in the system. The Lie bracket $ad_f g(q)$ is defined as $[f, g](q) = \frac{\partial g}{\partial q} f(q) - \frac{\partial f}{\partial q} g(q)$. For this system, $m = 2$.

The first condition, $\Delta = \text{span}\{g(q)\}$ is involutive because $[g, g] \in \Delta$ [39]. Proving the second condition requires that we compute $G(q) = [g(q), ad_f g(q)]$. In this case,

$$ad_f g(q) = -\frac{df(q)}{dq} \begin{bmatrix} -1 \\ 0 \end{bmatrix},$$

where

$$\frac{\partial f(q)}{\partial q} = \begin{bmatrix} \frac{\partial f_1(q)}{\partial \alpha} & \frac{\partial f_1(q)}{\partial \beta} \\ \frac{\partial f_2(q)}{\partial \alpha} & \frac{\partial f_2(q)}{\partial \beta} \end{bmatrix} = \begin{bmatrix} f_{1\alpha} & f_{1\beta} \\ f_{2\alpha} & f_{2\beta} \end{bmatrix}.$$

The derivative of the first element of f with respect to α is defined as $f_{1\alpha}$. Note that the Jacobian requires a partial derivative with respect to $q_2 = (\beta - \omega_0^{-1})$. However, since the derivatives are the same with respect to β , we use that variable to simplify the notation. The partial derivatives are defined as

$$\begin{aligned} f_{1\alpha} &= \beta^{-1}(-v_y \sin(\alpha + \theta) - v_x \cos(\alpha + \theta) + \cos(\alpha)) \\ f_{2\alpha} &= -v_x \sin(\alpha + \theta) + v_y \cos(\alpha + \theta) + \sin(\alpha) \\ f_{1\beta} &= -(\beta)^{-2}(v_y \cos(\alpha + \theta) - v_x \sin(\alpha + \theta) + \sin(\alpha)) \\ f_{2\beta} &= 0. \end{aligned}$$

The partial derivative of g with respect to q is

$$\frac{dg(q)}{dq} = 0.$$

Therefore,

$$ad_f g(q) = \begin{bmatrix} f_{1\alpha} \\ f_{2\alpha} \end{bmatrix},$$

and

$$G(q) = \begin{bmatrix} -1 & \beta^{-1}(-v_y \sin(\alpha + \theta) - v_x \cos(\alpha + \theta) + \cos(\alpha)) \\ 0 & -v_x \sin(\alpha + \theta) + v_y \cos(\alpha + \theta) + \sin(\alpha) \end{bmatrix}. \quad (3.15)$$

This matrix $G(q)$ is rank 2 if $f_1(q) = -v_x \sin(\alpha + \theta) + v_y \cos(\alpha + \theta) + \sin(\alpha) \neq 0$. There are two cases when $f_1(q) = 0$. First, when the UAV is moving at the same speed and has the same direction as the target. Under the assumption that the speed of the UAV is greater than speed of the target, this case cannot be true. Second, the cases where the UAV has one component of its velocity equal to the same component of the velocity of the target, i.e. $\dot{r}_x = v_x$ or $\dot{r}_y = v_y$. The UAV remains in this state only when $u = 0$, since v_x and v_y are constant. Figure 3.3 illustrates this case where $\dot{r}_x = v_x$, $\alpha + \theta = \frac{\pi}{2}$ and $\dot{r}_y \neq v_y$ since speed of the UAV is greater than the target. The dynamics for these cases are not invariant, as we will see in Equation (3.17). For the rest of the states of the system, $\text{rank}(G(q)) = 2$ and the system is feedback linearizable. Let $h(x) = q_2$ from Equation (3.13). We

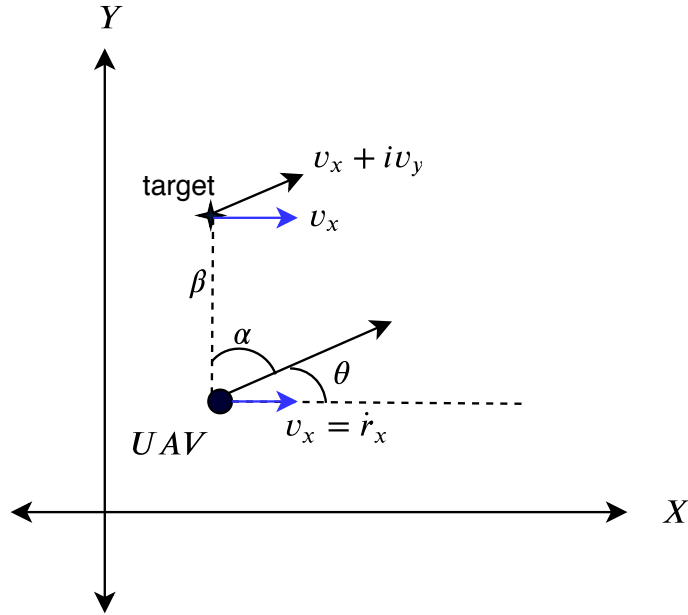


Figure 3.3: Figure that depicts transient cases where the matrix $G(q)$ is not full rank. This happens when one component, the X or the Y, of the velocity of the UAV and target are equal, and $\alpha + \theta = \pm \frac{\pi}{2}$. Here, the X component is equal and the UAV is directly below the target, with $\alpha + \theta = \frac{\pi}{2}$. This degenerate case could also occur if $\dot{r}_y = v_y$.

define the linearizable states as

$$\begin{aligned} z &= \begin{bmatrix} h(q) \\ L_f h(q) \end{bmatrix} \\ &= \begin{bmatrix} \beta - \omega_0^{-1} \\ v_x \cos(\alpha + \theta) + v_y \sin(\alpha + \theta) - \cos(\alpha) \end{bmatrix}, \end{aligned}$$

where $L_f h(q) = \frac{\partial h(q)}{\partial q} f(q)$ is the Lie derivative of h with respect to f . Driving z to zero drives β to the desired radius ω_0^{-1} and α to the desired angle for a circle around the moving target. Since $\dot{\beta}$ is a function of α , driving $\dot{\beta}$ to zero implicitly ensures that the α angle is driven to the desired value. Thus, driving these error states to zero will cause the UAV to encircle the constant velocity target. The derivatives of the error states with respect to time are

$$\begin{aligned} \dot{z}_1 &= \dot{\beta} \\ &= v_x \cos(\alpha + \theta) + v_y \sin(\alpha + \theta) - \cos(\alpha) \\ &= z_2, \\ \dot{z}_2 &= -v_x \sin(\alpha + \theta)(\dot{\alpha} + \dot{\theta}) + \sin(\alpha)\dot{\alpha} \\ &\quad + v_y \cos(\alpha + \theta)(\dot{\alpha} + \dot{\theta}). \end{aligned} \tag{3.16}$$

The error state dynamics become

$$\dot{z} = \begin{bmatrix} \dot{z}_1 \\ \dot{z}_2 \end{bmatrix} = \begin{bmatrix} z_2 \\ \beta(f_1^2(q)) - \sin(\alpha)u \end{bmatrix},$$

where $f_1(q)$ is given in Equation (3.14).

Theorem 2. *All trajectories of a UAV following the dynamics of Equations (2.1) and using the control law*

$$u = \frac{\beta(f_1^2(q)) - \eta}{\sin(\alpha)}, \tag{3.17}$$

where $\eta = -K_1 z_1 - K_2 z_2$ is the negated error states with gains $K_1 > 0$ and $K_2 > 0$ and f_1 defined in Equation (3.14), will globally exponentially converge to a circle with radius $\beta = \omega_0^{-1}$ around a

target moving with constant velocity and the speed of the target always less than the speed of the UAV.

Proof. With the proposed control, the error dynamics are

$$\dot{z} = \begin{bmatrix} z_2 \\ -K_1 z_1 - K_2 z_2 \end{bmatrix} = \begin{bmatrix} 0 & 1 \\ -K_1 & -K_2 \end{bmatrix} z.$$

Choosing $K_1 > 0$ and $K_2 > 0$ will ensure \dot{z} is exponentially stable and the control (Equation (3.17)) will drive the UAV to a constant radius circle around the moving target. The denominator goes to zero only when the UAV is pointing directly towards or away from the target, which is a subset of the cases described when $\text{rank}(G(q)) \neq 2$, and are transient due to the dynamics. The controller design does not let the UAV drive itself into such a scenario, since the controller pushes the UAV away from the center (the angular rate $u = \dot{\theta}$ pushes the UAV away so that α goes away from 0 or π), to achieve α oscillating near $\frac{\pi}{2}$ and the range $\beta = \omega_0^{-1}$. When the UAV starts at that position, or reaches it due to errors in measurements (Chapter 5), we saturate the control with a maximum value as in Equation (2.2), and it gets out of that state.

Thus the controller given in Equation (3.17) directs the UAV, which is following dynamics in Equation (2.1), to travel in a constant radius circle given by $\beta = \omega_0^{-1}$ around the constant velocity moving target, moving with speed less than the speed of the UAV.

□

Figure 3.4 shows convergence of the UAV trajectories to a loiter circle around a target moving with constant velocity. The blue line shows the motion of the target, with the dashed line showing the trajectory of the UAV. The pink “+” is the initial position of the UAV. The UAV encircles the target depending on the starting conditions, which in this case is counter-clockwise.

To gain intuition on how the encircling direction is determined, consider the control law $u = K_1(\beta - \omega_0^{-1}) + K_2(\dot{\beta})$, which is similar to a PD controller, where the sign of K_1 and K_2 (assuming both are same sign) determines whether the UAV will converge to a clockwise or counter-clockwise circle. In the controller proposed in Equation (3.17), there is a $\sin(\alpha)$ term dividing the PD portion of the controller. This cancels with the sign of K_1 and K_2 and ensures that UAVs moving in both the clockwise and counter-clockwise direction converge to a loiter circle. So although in the

case of positive gains K_1 and K_2 which exponentially stabilizes the circular trajectories, we are unable to control the direction of the convergence, since for both positive and negative α , we get convergence. This poses a number of problems, such as, collision avoidance becomes difficult, UAVs cannot maintain a formation following each other, and coordinate frames for information exchange and estimation may be reversed. The following section proposes a controller which provides direction control.

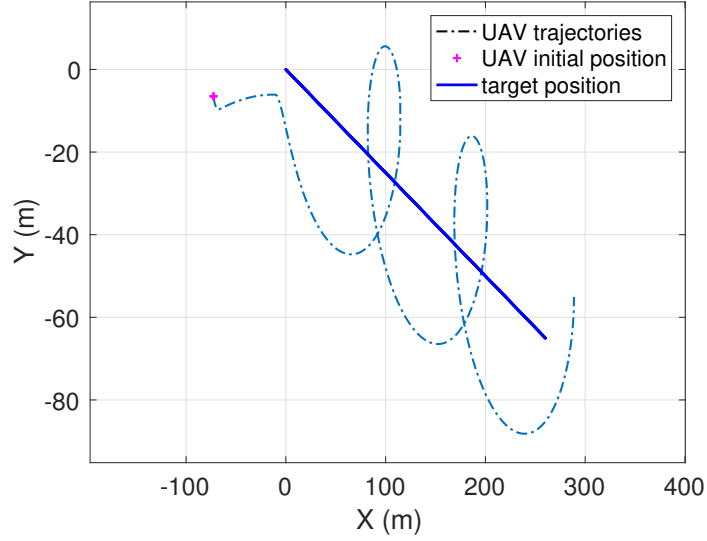


Figure 3.4: Constant velocity target encirclement. Velocity of the target is $v_x + iv_y = 0.4 - i0.1m/s$.

3.3 Direction Control While Encircling Constant Velocity Targets

In this section, we present a controller which enables us to specify the direction of encirclement for a constant velocity target. The controller in the previous section does not allow control of the direction of encirclement. We know that when the UAV is on the circle with radius ω_0^{-1} , $\dot{\beta} = 0$. Using Equation (3.11) for range-rate $\dot{\beta} = 0$, we get

$$\tan(\alpha) = \frac{1 - v_x \cos(\theta) - v_y \sin(\theta)}{v_y \cos(\theta) - v_x \sin(\theta)}. \quad (3.18)$$

Therefore the desired relative angle α_d , when the range-rate is zero, is given by

$$\alpha_d = \text{atan2}\left(d(1 - v_x \cos(\theta) - v_y \sin(\theta)), d(v_y \cos(\theta) - v_x \sin(\theta))\right) = \text{atan2}\left(d\alpha_y, d\alpha_x\right), \quad (3.19)$$

where α_x and α_y are the X and Y components of the vector defining the angle α_d and d defines the direction, with $d = -1$ being clockwise and $d = +1$ being counter-clockwise. Note that we do not cancel out d from the fraction in order to specify the quadrant of the angle α for atan2 .

Consider the error state vector

$$e = \begin{bmatrix} \beta - \omega_0^{-1} \\ \alpha - \alpha_d \end{bmatrix}. \quad (3.20)$$

Its derivative with respect to time is

$$\dot{e} = \begin{bmatrix} \dot{\beta} \\ \dot{\alpha} - \dot{\alpha}_d \end{bmatrix} = \begin{bmatrix} v_x \cos(\alpha + \theta) + v_y \sin(\alpha + \theta) - \cos(\alpha) \\ \frac{A}{\beta} - u \left(\frac{\alpha_y}{\alpha_x^2 + \alpha_y^2} \right) \end{bmatrix}, \quad (3.21)$$

where

$$A = v_y \cos(\alpha + \theta) - v_x \sin(\alpha + \theta) + \sin(\alpha). \quad (3.22)$$

Theorem 3. *All trajectories of a UAV following the dynamics of Equations (2.1) and using the control law*

$$u = \frac{\alpha_x^2 + \alpha_y^2}{\alpha_y} \left(\frac{A}{\beta} + \frac{(\beta - \omega_0^{-1})\dot{\beta}}{\alpha - \alpha_d} + K_1(\beta - \omega_0^{-1})^2(\alpha - \alpha_d) + K_2(\alpha - \alpha_d) \right), \quad (3.23)$$

will globally asymptotically converge to a circle with radius $\beta = \omega_0^{-1}$ around a target moving with constant velocity and the speed of the target less than the speed of the UAV.

Proof. Using error states from Equation (3.20), we take the Lyapunov function as $V = \frac{1}{2}e^H e$. The derivative is thus $\dot{V} = \text{real}(e^H \dot{e})$, given by

$$\dot{V} = (\beta - \omega_0^{-1})\dot{\beta} + \left(\frac{A}{\beta} \right) (\alpha - \alpha_d) - u(\alpha - \alpha_d) \left(\frac{\alpha_y}{\alpha_x^2 + \alpha_y^2} \right).$$

The set where the derivative of the Lyapunov function is zero is $S = \{(e, 0), (0, \dot{e}), (0, 0)\}$.

We define the largest invariant set $E \subset S$, with $E = \{(0,0)\}$. We know in E , $\dot{e} = 0$. Thus $\dot{e}_1 = \dot{\alpha} - \dot{\alpha}_d = 0$ and $\dot{e}_2 = \dot{\beta} = 0$. This shows β is a constant, and also by definition of α_d in Equation (3.19), we get $\alpha = \alpha_d$. Substituting these values in the control from Equation (3.23) yields

$$u = \frac{\alpha_x^2 + \alpha_y^2}{\alpha_y} \left(\frac{A}{\beta} + (\beta - \omega_0^{-1}) \right).$$

Substituting this control u in $\dot{e}_2 = \dot{\alpha} - \dot{\alpha}_d = 0$, results in $\beta = \omega_0^{-1}$. Thus, in Equation (3.20), $e = 0$. Therefore trajectories that start in the set E stay in E and $E = \{(0,0)\}$ is invariant.

According to the Lasalle's invariance theorem ([39], Theorem 4.4, Corollary 4.1), the controller is globally asymptotically stable in driving the error states to zero. This implies that it drives β to ω_0^{-1} and α to α_d asymptotically, which are the conditions necessary to drive a UAV to encircle a target moving with constant velocity at a radius of ω_0^{-1} . \square

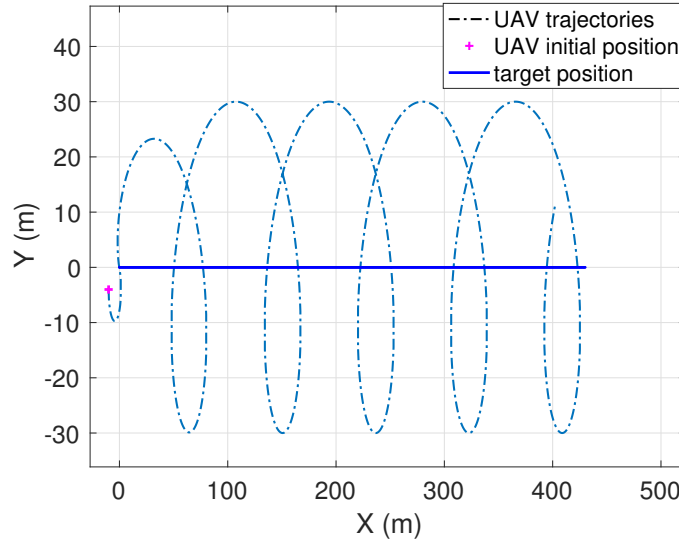


Figure 3.5: Target encirclement in clockwise direction for target moving with velocity $v_x = 0.4m/s$.

Figure 3.5 shows convergence of the UAV in clockwise direction. The UAV initially started going in the counter-clockwise direction, but is forced to converge in the clockwise direction with $d = -1$. The dashed lines denote the UAV trajectory and the blue line denotes the motion of the target. The pink “+” marks the UAV initial position. The radius is set to $\omega_0^{-1} = 30m$.

3.4 Encirclement of Constantly Accelerating Targets

In this section, we extend the feedback linearization controller from Section 3.2 to find an exponentially stable controller to encircle targets moving with constant acceleration. We assume that although the speed of the target is constantly changing, it still remains less than the speed of the UAV. The linearization approach carries over from the constant velocity controller, except the derivatives of the error states with respect to time change. We use the feedback linearizable states from Equation (3.16) as

$$\begin{aligned} z &= \begin{bmatrix} h(q) \\ L_f h(q) \end{bmatrix} \\ &= \begin{bmatrix} \beta - \omega_0^{-1} \\ v_x \cos(\alpha + \theta) + v_y \sin(\alpha + \theta) - \cos(\alpha) \end{bmatrix}, \end{aligned}$$

where $L_f h(q) = \frac{\partial h(q)}{\partial q} f(q)$. Driving z to zero drives β to the desired radius ω_0^{-1} and α to the desired relative angle for a UAV to encircle the target moving with constant acceleration and speed less than one. In the case of an accelerating target, the derivatives of the error states, differently from Equation (3.16) are

$$\begin{aligned} \dot{z}_1 &= \dot{\beta} \\ &= v_x \cos(\alpha + \theta) + v_y \sin(\alpha + \theta) - \cos(\alpha) \\ &= z_2, \\ \dot{z}_2 &= -v_x \sin(\alpha + \theta)(\dot{\alpha} + \dot{\theta}) + \sin(\alpha)\dot{\alpha} \\ &\quad + v_y \cos(\alpha + \theta)(\dot{\alpha} + \dot{\theta}) \\ &\quad + a_x \cos(\alpha + \theta) + a_y \sin(\alpha + \theta). \end{aligned}$$

Thus, the error state dynamics become

$$\dot{z} = \begin{bmatrix} \dot{z}_1 \\ \dot{z}_2 \end{bmatrix} = \begin{bmatrix} z_2 \\ \beta(f_1^2(q)) - \sin(\alpha)u + a_x \cos(\alpha + \theta) + a_y \sin(\alpha + \theta) \end{bmatrix}, \quad (3.24)$$

where $f_1(q)$ is given in Equation (3.14).

Theorem 4. All trajectories of a UAV following the dynamics of Equations (2.1) and using the control law

$$u = \frac{\beta(f_1^2(q)) + a_x \cos(\alpha + \theta) + a_y \sin(\alpha + \theta) - \eta}{\sin(\alpha)}, \quad (3.25)$$

where $\eta = -K_1 z_1 - K_2 z_2$ is the negated error states with gains $K_1 > 0$ and $K_2 > 0$ and f_1 defined in Equation (3.14), will globally exponentially converge to a circle with radius $\beta = \omega_0^{-1}$ around a target moving with constant acceleration and the speed of the target always less than the speed of the UAV.

Proof. With this control, the error dynamics are

$$\dot{z} = \begin{bmatrix} z_2 \\ -K_1 z_1 - K_2 z_2 \end{bmatrix} = \begin{bmatrix} 0 & 1 \\ -K_1 & -K_2 \end{bmatrix} z.$$

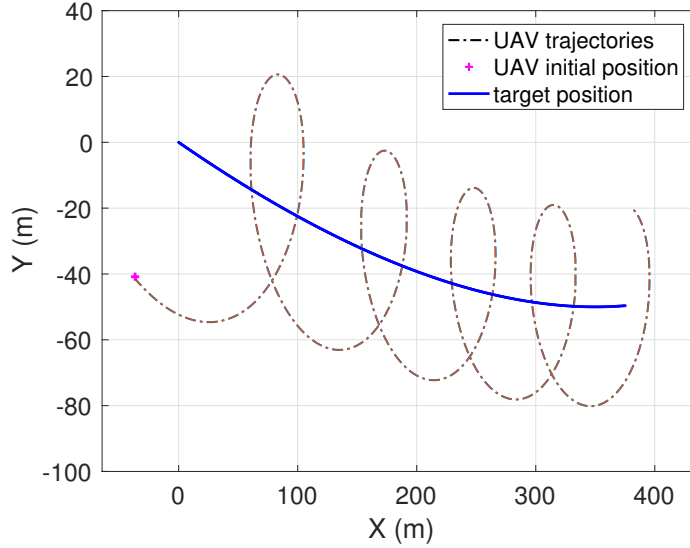


Figure 3.6: Encirclement of a constantly accelerating target with $a_x + ia_y = (-0.0001 + i0.0001)m/s^2$ and initial velocity $v_x + iv_y = (0.4 - i0.1)m/s$.

Choosing $K_1 > 0$ and $K_2 > 0$ will ensure \dot{z} is exponentially stable and the control (Equation (3.25)) will drive the error states to zero which are the conditions for a UAV to encircle a target moving with constant acceleration with constant radius ω_0^{-1} . The denominator of the control goes to zero only when the UAV is pointing directly towards or away from the target, which is a subset

of the cases described when $\text{rank}(G(q)) \neq 2$ (Section 3.2), and are transient due to the dynamics. This case is depicted in Figure 3.3 and discussed in the proof of Theorem 3.2. \square

Figure 3.6 shows the convergence of the UAV (dashed lines) to a loiter circle of radius 30m around the constantly accelerating target (blue line), with acceleration $a_x + ia_y = (-0.0001 + i0.0001)m/s^2$. The pink “+” marks the initial position of the UAV. The direction is decided by the initial position and heading of the UAV which is counter-clockwise in this case.

3.5 Direction Control While Encircling Constant Acceleration Targets

Following the rationale from the directional controller for constant velocity targets in Section 3.3, we include acceleration in the formulation. For the error in Equation (3.20), the new error dynamics are defined as

$$\dot{e} = \begin{bmatrix} \dot{\beta} \\ \dot{\alpha} - \dot{\alpha}_d \end{bmatrix} = \begin{bmatrix} v_x \cos(\alpha + \theta) + v_y \sin(\alpha + \theta) - \cos(\alpha) \\ \frac{A}{\beta} - u \left(\frac{\alpha_y}{\alpha_x^2 + \alpha_y^2} \right) + \frac{v}{\alpha_x^2 + \alpha_y^2} \end{bmatrix}, \quad (3.26)$$

where $v = \alpha_x(a_x \cos(\theta) + a_y \sin(\theta)) + \alpha_y(a_y \cos(\theta) - a_x \sin(\theta))$ are the acceleration terms, and A is defined as in Equation (3.22).

Theorem 5. *All trajectories of a UAV following the dynamics of Equations (2.1) and using the control law*

$$u = \frac{\alpha_x^2 + \alpha_y^2}{\alpha_y} \left(\frac{A}{\beta} + \frac{(\beta - \omega_0^{-1})\dot{\beta}}{\alpha - \alpha_d} + K_1(\beta - \omega_0^{-1})^2(\alpha - \alpha_d) + K_2(\alpha - \alpha_d) \right) + \frac{v}{\alpha_y}, \quad (3.27)$$

will globally asymptotically converge to a circle with radius $\beta = \omega_0^{-1}$ around a target moving with constant acceleration and the speed of the target always less than the speed of the UAV.

Proof. Using error states from Equation (3.20), we take the Lyapunov function as $V = \frac{1}{2}e^H e$. Differentiating with respect to time yields

$$\dot{V} = \text{real}(e^H \dot{e}) = (\beta - \omega_0^{-1})\dot{\beta} + \left(\frac{A}{\beta} + \frac{v}{\alpha_x^2 + \alpha_y^2} \right) (\alpha - \alpha_d) - u(\alpha - \alpha_d) \left(\frac{\alpha_y}{\alpha_x^2 + \alpha_y^2} \right).$$

The set where the derivative of the Lyapunov function is zero is $S = \{(e, 0), (0, \dot{e}), (0, 0)\}$. We define the largest invariant set $E \subset S$, with $E = \{(0, 0)\}$. We will show that this is the largest invariant set. We know in E the dynamics must be zero. For dynamics $\dot{e} = 0$, $\dot{e}_1 = \dot{\alpha} - \dot{\alpha}_d = 0$ and $\dot{e}_2 = \dot{\beta} = 0$. This shows β is a constant, and also by definition of α_d in Equation (3.19), we get $\alpha = \alpha_d$. Substituting these values in the control from Equation (3.27), we get

$$u = \frac{\alpha_x^2 + \alpha_y^2}{\alpha_y} \left(\frac{A}{\beta} + (\beta - \omega_0^{-1}) \right) + \frac{v}{\alpha_y}. \quad (3.28)$$

Substituting Equation (3.28) in $\dot{\alpha} - \dot{\alpha}_d = 0$ from Equation (3.26), we get $\beta = \omega_0^{-1}$. Thus, in Equation (3.20), $e = 0$. Therefore trajectories that start in set E , stay in the set E , and the set $E = \{(0, 0)\}$ is the largest invariant set. According to Lasalle's invariance theorem ([39], Theorem 4.4, Corollary 4.1), the controller is globally asymptotically stable in driving the error states to zero. Thus, it drives β to ω_0^{-1} and α to α_d , which are the conditions necessary to drive a UAV to encircle a target moving with constant acceleration and speed less than one, at a radius of ω_0^{-1} . \square

Figure 3.7 shows convergence of the UAV (dashed) to a clockwise circle of radius 30m around a constantly accelerating target (solid). The pink "+" shows the initial position of the UAV.

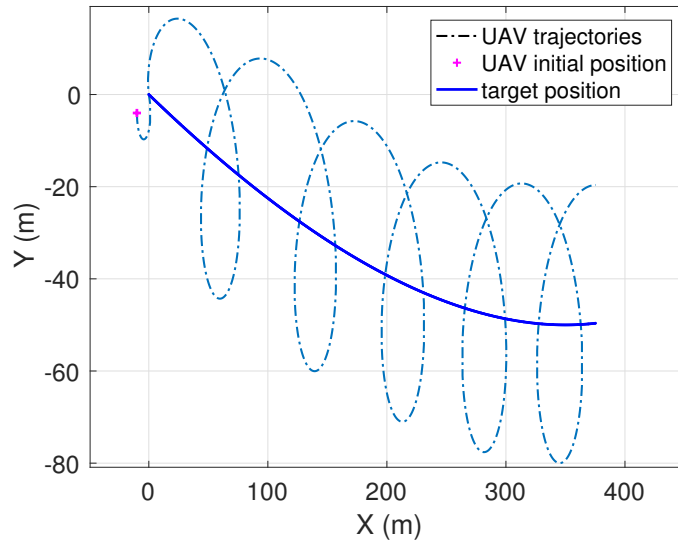


Figure 3.7: Target encirclement in clockwise direction for target moving with initial velocity $v_x + iv_y = (0.4 - i0.1)m/s$ and acceleration $a_x + ia_y = (-0.0001 + i0.0001)m/s^2$.

CHAPTER 4. MULTI-AGENT COORDINATION

For more efficient completion of tasks with better coverage of the task area, communication and coordination is important among all the UAVs performing the tasks. In this chapter, we discuss two different approaches: The first arrangement of UAVs to a desired formation, and the second for multi-UAV communication in large systems.

First, we define a method to arrange the UAVs in a symmetric formations in a circle around the target, specifically the temporally equi-spaced (time-splay) formation. Using the controller proposed in 3, and inspired from the work in [29], [32], we explore the arrangement of UAVs in symmetric formations using the relative frame information. Splay formations help in providing good coverage of a target [40].

We also discuss a way to relay information between multiple groups of UAVs. Using messenger UAVs, we discuss the effect of sending UAVs at a higher frequency between groups on information spread time within the whole system. This approach is useful when the groups of UAVs are too far apart to communicate directly, such as in search missions over oceans or forests. Previous works [34], [35] have discussed information sharing using gossip algorithms among nearby robots in search tasks. Taking inspiration from the epidemic model in [33] and work in [34], [35], we study the bounds on time-to-spread information in a system with multiple groups of robots encircling targets.

4.1 Time-Splay Formations

In a constant velocity moving target scenario, the UAVs must turn at different rates around different parts of the circle, to be able to maintain a constant distance from the target, i.e., $\dot{\theta}_k \neq$ constant, which is different from the stationary target case. In case of stationary targets, equi-temporal-spacing is equivalent to equal spatial distance, but it is different in case of moving targets. Our aim is to arrange the UAVs around the target in a circle such that they are temporally equi-

distant from each other, i.e., at any instant, an observer on the circle would see the UAVs pass at a constant rate. This helps us have more robust tracking and re-arrangement in case of UAV attrition or addition. In this section, to arrange the UAVs in a time-splay formation, we build upon the work from [1], [29], [32], which assume inertial frame information for the UAVs and the target. The proposed controller arranges the UAVs in locally stable circularly symmetric states. The different symmetric states are: Symmetric: time-splay, Coordinated: all on top of each other, and everything in between – clubbed as two vehicles on each spot, three on each spot, etc, dependant on how many formations can exist for the given number of UAVs. An example is shown in Figure 4.1. Depending on the gain K_{splay} in Equation (4.11) and initial conditions, we can control which symmetric state we end up in. We are interested in the time-splay state, where the UAVs are spread around the circle, and is thus more practically useful.

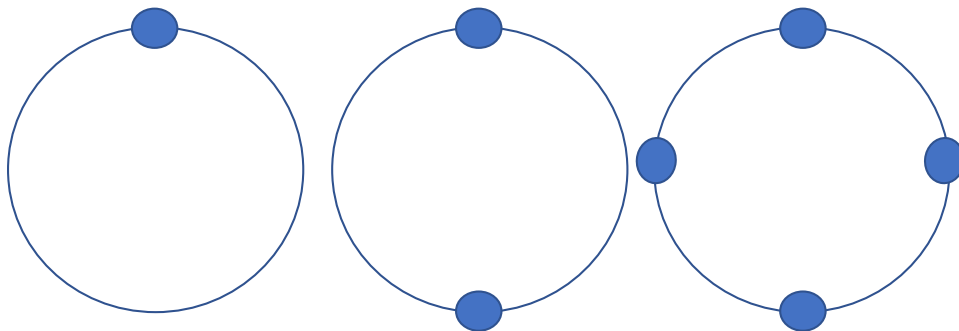


Figure 4.1: Different symmetric formations for a four UAV scenario in a stationary target case: (left) Coordinated, (middle) Two-tuple, (right) Symmetric. See also [1].

As in the previous chapter, the information known to the UAVs about the target is the range β_k , the bearing to the target α_k , and their own local heading angle θ_k . We also assume a constant velocity UAV, with just commanding the turn-rate, and assume the speed of the UAV is greater than that of the target. To maintain a symmetric formation amongst the encircling UAVs, we need a metric to track where the UAV is on the circle around the target. Although α_k is periodic, we cannot use it as the metric, since the position on the circle and the bearing α_k do not have a one-to-one mapping, i.e., there are multiple positions on the circle with the same value of α_k . We cannot use θ_k directly either, since the frame of reference of the measurement of θ_k is different for each of the UAVs.

We know that for every UAV_k with their local bearing θ_k , there is an angle of the target motion $\psi_k = \tan^{-1}\left(\frac{v_{y_k}}{v_{x_k}}\right)$ in their local frame. Since each UAV has its own reference frame, we use the vector of the relative motion of the UAV with respect to the target's motion frame for achieving the symmetric formations. Let $\gamma_k = \arg(e^{i\theta_k} - ve^{i\psi_k})$ be the relative heading of the UAV_k in the moving target frame, where v is the speed of the target. Since this frame is common for all UAVs (assuming no noise), γ_k may be used to track the progress around the circle. The speed of the UAV in the target frame is defined as $s_k = |e^{i\theta_k} - ve^{i\psi_k}|$, where $|\cdot|$ denotes the magnitude. For this section, we assume a target moving only in the X direction, without any loss of generality, as the direction of motion for a constant velocity target is just a function of the frame of reference. The relationship between $\dot{\gamma}_k$ and the control u_k is obtained by differentiating $\gamma_k = \arg(e^{i\theta_k} - ve^{i\psi_k})$ with respect to time to get

$$\dot{\gamma}_k = \frac{1 - v\cos(\theta_k)}{s_k^2} \dot{\theta}_k. \quad (4.1)$$

We define which UAVs communicate with each other, using the Laplacian topology matrix $L_{N \times N}$ for the N UAVs in formation. The diagonal element L_{kk} represents how many other UAVs are connected to the k^{th} UAV, and the row elements $L_{kl} = -1$ for every UAV_l that UAV_k is connected to. We assume bi-directional connections and thus the matrix is symmetric. As an example topology, we consider a ring topology, where each UAV is able to communicate with the UAVs immediately preceding and following it in the graph, as in [1]. Note that this topology is static and does not represent a spatially constructed ring. For a seven UAV scenario, L is given by

$$L = \begin{bmatrix} 2 & -1 & 0 & 0 & 0 & 0 & -1 \\ -1 & 2 & -1 & 0 & 0 & 0 & 0 \\ 0 & -1 & 2 & -1 & 0 & 0 & 0 \\ 0 & 0 & -1 & 2 & -1 & 0 & 0 \\ 0 & 0 & 0 & -1 & 2 & -1 & 0 \\ 0 & 0 & 0 & 0 & -1 & 2 & -1 \\ -1 & 0 & 0 & 0 & 0 & -1 & 2 \end{bmatrix}. \quad (4.2)$$

The time period T for a UAV to encircle the moving target once is defined as [32]

$$T = \frac{1}{\omega_0} \int_0^{2\pi} \frac{d\gamma_k}{s_k}. \quad (4.3)$$

The time phase ϕ_k is defined in [32] as

$$\phi_k = \frac{2\pi}{\omega_0 T} \int_0^{\gamma_k} \frac{d\gamma_k}{s_k}, \quad (4.4)$$

and is a measure of how far the UAV has progressed around the circle.

As was done in [29], we add a rotationally symmetric potential U to the potential function $V = \frac{1}{2}e^H e$, where e is defined in Equation (3.20). The rotationally symmetric potential is defined as $U = \sum_{m=1}^M K_m U_m$, with $U_m = \frac{N}{2} |p_m|^2$ and $p_m = \frac{1}{mN} \sum_{k=1}^N e^{im\phi_k}$, and is symmetric around the circle with respect to ϕ_k . The symmetric potential U is thus defined as

$$U = \sum_{m=1}^M K_m \frac{1}{2m^2 N} \left| \sum_{k=1}^N e^{im\phi_k} \right|^2. \quad (4.5)$$

The potential U is rotationally symmetric, i.e., $U(\gamma_k(t)) = U(\gamma_k(t - \frac{T}{N}))$, where $U(\gamma_k(t))$ is the value of the potential evaluated with the value of γ_k at time t . The augmented Lyapunov potential function is

$$V_{splay} = V + \frac{T}{2\pi} U. \quad (4.6)$$

Thus we get the derivative of the potential function

$$\dot{V}_{splay} = \dot{V} + \frac{T}{2\pi} \frac{\partial U}{\partial \phi_k} \dot{\phi}_k, \quad (4.7)$$

where \dot{V} is the time derivative of the potential function from Equation (3.3) and

$$\dot{\phi}_k = \frac{2\pi}{T} (\omega_0 s_k)^{-1} \dot{\gamma}_k. \quad (4.8)$$

Thus, we get the time derivative of the augmented potential function as

$$\begin{aligned} \dot{V}_{splay} = & (\beta_k - \omega_0^{-1})\dot{\beta}_k + \left(\frac{A_k}{\beta_k}\right)(\alpha_k - \alpha_{k_d}) - u(\alpha_k - \alpha_{k_d}) \left(\frac{\alpha_{k_y}}{\alpha_{k_x}^2 + \alpha_{k_y}^2}\right) \\ & + (\omega_0 s_k)^{-1} \frac{\partial U}{\partial \phi_k} \frac{(1 - v \cos(\theta_k))}{s_k^2} u_k. \end{aligned} \quad (4.9)$$

The partial of the rotationally symmetric potential U with respect to ϕ_k [1] is defined as

$$\frac{\partial U}{\partial \phi_k} = \text{real}([(ie^{i\phi}) \circ Le^{i\phi}]_k), \quad (4.10)$$

where $(\bar{\cdot})$ denotes a complex conjugate, \circ denotes a Hadamard product (or element-wise product) [41], and $[\cdot]_k$ denotes the k^{th} element of the vector in the square brackets. This derivative goes to zero when $\dot{\phi}_k$ is a constant and the vehicles are in a symmetric state.. Thus, the potential U is a constant when $\dot{\phi}_k$ is a constant, and is minimized when the UAVs arrange themselves in a symmetric formation around the circle [1].

Theorem 6. *All trajectories of the UAVs following the dynamics of Equations (2.1) and using the control law*

$$\begin{aligned} u_{splay_k} = & \frac{s_k^2(\alpha_k - \alpha_{k_d})}{(1 - v \cos(\theta_k))((\alpha_k - \alpha_{k_d}) - \frac{\partial U}{\partial \phi_k} / \omega_0 s_k)} \left(\frac{A}{\beta_k} + \frac{(\beta_k - \omega_0^{-1})\dot{\beta}_k}{\alpha_k - \alpha_{k_d}} + \right. \\ & \left. K_1(\beta_k - \omega_0^{-1})^2(\alpha_k - \alpha_{k_d}) + K_2(\alpha_k - \alpha_{k_d}) \right) + K_{splay} \frac{(1 - v \cos(\theta_k))((\alpha_k - \alpha_{k_d}) - \frac{\partial U}{\partial \phi_k} / \omega_0 s_k)}{s_k^2} \end{aligned} \quad (4.11)$$

will globally asymptotically converge to a circle with radius $\beta = \omega_0^{-1}$ around a target moving with constant velocity whose speed is always less than the speed of the UAV, while arranging the UAVs in a locally symmetric formation around the circle.

Proof. Substituting the control law from Equation (4.11) into the Equation (4.9), gives $\dot{V}_{splay} = -K_1(\beta_k - \omega_0^{-1})^2(\alpha_k - \alpha_{k_d})^2 - K_2(\alpha_k - \alpha_{k_d})^2 - K_{splay} \left(\frac{(1 - v \cos(\theta_k))((\alpha_k - \alpha_{k_d}) - \frac{\partial U}{\partial \phi_k} / \omega_0 s_k)}{s_k^2} \right)^2$, which is a negative semi-definite function, and $\dot{V}_{splay} = 0$ when $\alpha_k = \alpha_{k_d}$ and $\frac{\partial U}{\partial \phi_k} = 0$, for all values of β_k .

Following the proof of Theorem3.3, we know that driving $\alpha_k = \alpha_{k_d}$ drives the UAV to a constant radius circle with $\beta_k = \omega_0^{-1}$. For this, error e in Equation (3.20) is zero, and $\dot{e} = 0$, which

means we are on circle and the derivative of the potential becomes $\dot{V}_{splay} = \frac{1}{\omega_0 s_k^3} \frac{\partial U}{\partial \phi_k}$. Thus, when we are on the circle, $\dot{V}_{splay} = 0$ only when $\frac{\partial U}{\partial \phi_k} = 0$. From Equation (4.10), we get ϕ_k is a constant when the derivative of the symmetric potential is zero. This is also supported by the fact that $\dot{\gamma}_k = \omega_0 s_k$ when going on a circle, and thus $\dot{\phi}_k = \frac{2\pi}{T}$ in Equation (4.8), which is a constant. The set $S = \{\dot{V}_{splay} = 0\}$ is invariant only at the origin $E = \{(e = 0, \dot{e} = 0, \frac{\partial U}{\partial \phi_k} = 0)\}$.

Thus, according to the Lasalle's invariance theorem ([39], Theorem 4.4, Corollary 4.1), the controller is globally asymptotically stable in driving the error states to zero, and thus UAVs to a constant radius circle around the moving target, while arranging the UAVs in a symmetric formation. Note that there are multiple symmetric formations for which $\frac{\partial U}{\partial \phi_k} = 0$, each of which are locally stable. □

Note that the splay state has a large region of attraction but there are cases when the UAVs arrange themselves in different symmetric states, including synchronized formations, i.e. on top of each other, etc. Analysis of when the UAVs enter which of these formations will be addressed in future work. For the time-splay formation shown in Figure 4.2, the gain of $K_{splay} = -N$ is chosen, where N is the number of UAVs [29].

Figure 4.2 (left) shows the UAVs in an inertial frame around the constant velocity target converging to the time-splay formation. Figure 4.2(right) shows the angle γ_k varying uniquely (but not linearly) in the range $[-\pi, \pi]$. We can see that in this figure that the UAVs slowly arrange themselves such that the phases don't overlap, but are equi-spaced, i.e., the distance between the angles in the horizontal axis is constant. This happens in the time-splay formations.

4.2 Gossip Algorithms for Inter-Group Communication

In a scenario with multiple targets being tracked by multi groups of UAVs, or multiple groups of vehicles searching a large area, inter-group communication enables the task to be executed in a more homogenous and efficient manner. In [35], the authors propose a method for information exchange in a multi-UAV routing problem using gossip algorithms. Inspired from this, we use the epidemic spread model from [33] to study the how information spreads among different groups and what are the upper bounds on the time to spread information to all the UAVs.

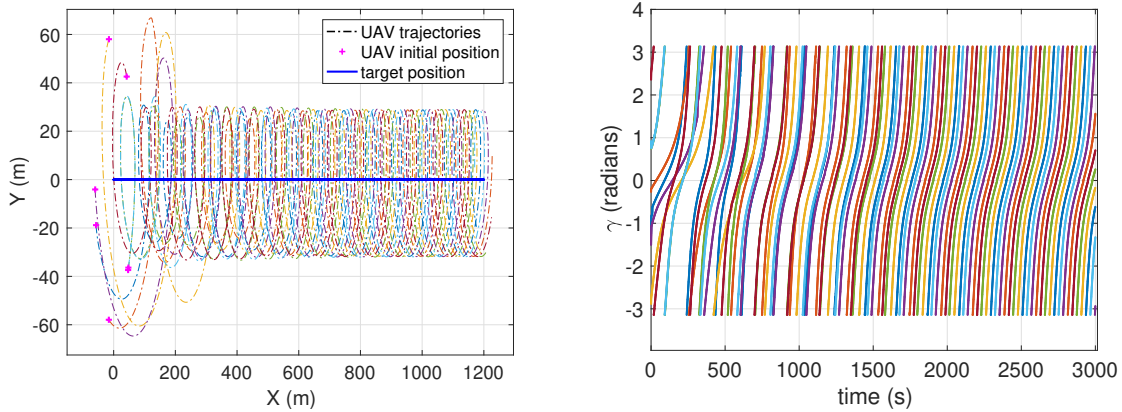


Figure 4.2: (left) Seven UAVs in the inertial frame in a time-splay formation around a constant velocity target moving with velocity $v_x + iv_y = (0.4)$ m/s and (right) the local angle γ_k of the UAV evolving from random positions to a time-splay formation.

We test how quickly information spreads among groups using a scenario with five different groups encircling five different stationary targets, as shown in Figure 4.3. We assume a common frame for all the UAVs and the targets, and assume all UAVs know the position of all the groups in the system. We set up communication between n groups by assigning a probability to every UAV to leave a group and go to another. The probability at every time step for a UAV to leave group i is μ_i and it chooses amongst the $n - 1$ groups with equal probability $\rho = \frac{1}{n-1}$. Differently from [33], which looks at heterogenous groups of agents, and thus consider both joining and leaving probabilities for each group, we are interested only in the leaving probability of the UAV from a group, since all UAVs are equivalent.

We can find the upper time bound on the information dissipation using this approach of sending UAVs from one group to another, where groups are farther than the communication range of the UAVs. The placement of the groups can affect how quickly the information dissipates. For example, if all the groups are in a straight line, the movement of one UAV from the first to the last group will make it encounter the rest of the groups, and the information will spread quickly. If all the groups are in a star or ring formation, the UAVs will not encounter other groups while travelling, providing a worst-case scenario. To get the upper bounds on time for the information spread throughout the system, we consider evenly spaced ring formation for our simulations.

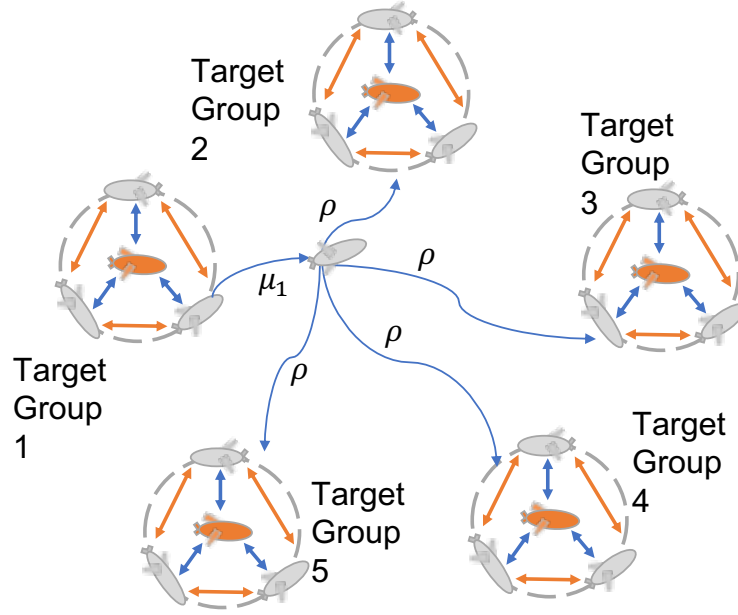


Figure 4.3: Mobility process linking five groups of UAVs with an example three UAVs in every group, μ_i is the probability at every time step for a UAV to leave group i . Denoted is an example with UAV leaving Group 1. $\rho = \frac{1}{n-1} = \frac{1}{4}$ is the probability that a person who leaves region i travels to region j , which is evenly distributed for all other four groups.

Group mobility can be expressed in terms of the number of UAVs moving between different groups as

$$\frac{dN_i}{dt} = \sum_j \frac{\mu_j}{n-1} N_j - \mu_i N_i, \quad (4.12)$$

where N_i is the number of UAVs in group i . This describes how the group sizes are changing, based on UAVs leaving and joining the group i . Groups with positive mobility have more vehicles joining them than leaving, and vice versa. Note that the group mobility can be low even when a lot of UAVs are joining and leaving the groups simultaneously.

Each UAV interacts with UAVs in a circular region of 50m, exchanging the following information about itself: ID, position, velocity, circle center (target position) of former and current group, IDs of other UAVs in it's former and current group, and the time instance of the information.

We will evaluate how quickly the information is spread to all the UAVs using Monte Carlo simulations. In the simulations, new information is given to a single UAV and the time-to-spread this information throughout the system of five groups is recorded. We use the stationary target tracker, and add the ability to send UAVs to different groups, depending on the probability of group

movement, μ_i . We assume the group positions are known to the UAVs. Once a UAV leaves its group (referred to as messenger UAV), it may encounter new UAVs, until it encounters somebody from the group it is supposed to join. In this venture, all the UAVs who come in contact with the messenger UAV exchange information with it, getting the latest information. This messenger UAV follows the new group, until it leaves again with probability μ_i .

We ran 100 simulations for each value of μ_i which varies from 0.00004 to 0.0012 in steps of 0.00004, i.e., the probability that any UAV leaves a group at any time step (every $\frac{1}{100}$ th of a second) varies from 0.00004 to 0.0012. We record the time taken for the information to spread over the whole system, with multiple groups and plot the mean and standard deviation over the 100 runs for each value of μ_i . There were five groups distributed in a star formation with five vehicles per group (initially).

Figure 4.4 shows the distribution of the time taken for information to spread compared with probability μ_i . We can see that after a certain movement probability, the time it take to spread the information plateaus, and we do not need to send the UAVs more frequently between groups. The scale of the graph would vary for different applications, but the qualitative trend of the time for dissipation of information vs the probability of leaving the groups would be the same.

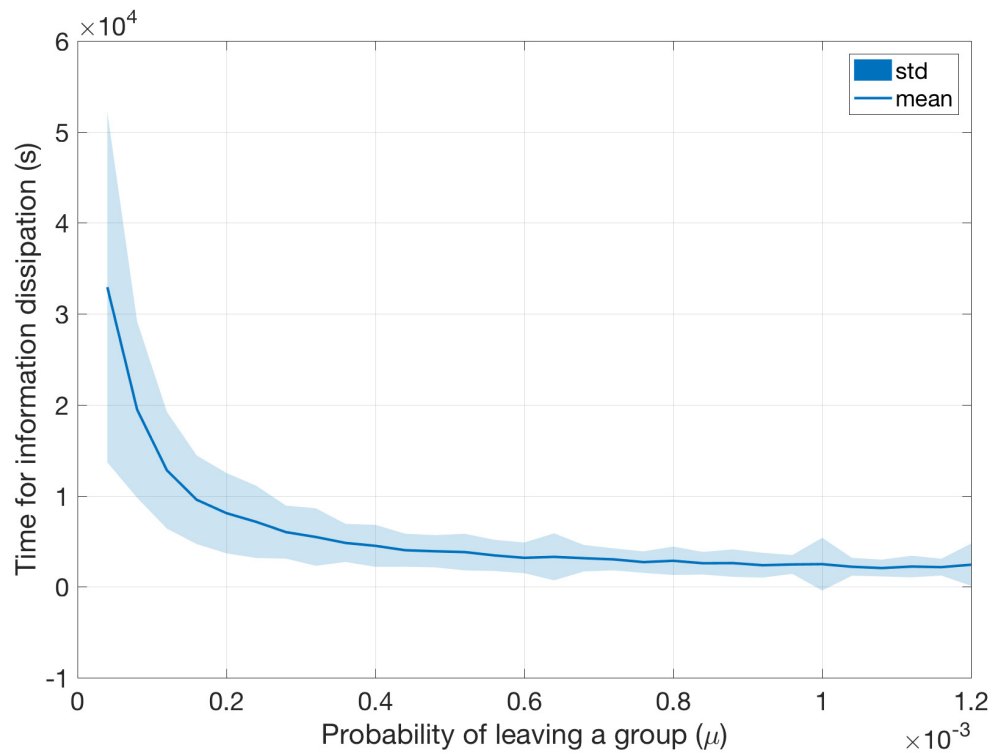


Figure 4.4: Time for information dissipation decreases with increasing probability of movement between groups. The x-axis denotes the probability of movement of UAVs between groups, and y-axis shows the time-to-spread the information, which is averaged over 100 simulation runs.

CHAPTER 5. ENCIRCLEMENT USING ONLY RELATIVE MEASUREMENTS: NOISE CONSIDERATIONS AND ESTIMATION

Thus far we have assumed noise-free measurements of the target and perfect knowledge of its velocity and/or acceleration. This is unrealistic for application in real-world scenarios. So in this section, we propose a framework using an Extended Kalman Filter (EKF) to estimate the non-linear states of the system. We estimate the measured states, α_k , β_k , along with their derivatives. We also estimate the local heading angle of each UAV, θ_k . We assume Gaussian noise in our measurements.

5.1 Noise Considerations

Cameras are a typical UAV sensor because of their low cost and weight and the ever-improving computer vision techniques available for detection and tracking of objects in images. Using monocular vision on a UAV, a depth estimate of the target can be obtained with a standard deviation of 3m [12] from the true depth. Thus, the standard error deviation for range measurements β_k is defined to be 3m. The error in bearing depends on the error in the detection of the target in the camera, and the errors in the attitude of the aircraft. Adding the standard deviations from [12] in yaw and azimuth measurements of the target (being more conservative, so not taking the square root), we assume $\pi/120$ rad standard deviation in error for bearing measurements α_k . We use these noisy measurements for encirclement of a target in the local frame of the UAV.

For the EKF, the error covariance matrix is initialized to $P = 10 I_{5 \times 5}$, where $I_{5 \times 5}$ is the identity matrix of size 5×5 . The covariance of the measurement noise is

$$R = \begin{bmatrix} (\pi/120)^2 & 0 \\ 0 & (3)^2 \end{bmatrix},$$

and the process noise is [42]

$$Q = \begin{bmatrix} \frac{\pi}{9} \frac{\Delta t^2}{3} & 0 & \frac{\pi}{9} \frac{\Delta t}{2} & 0 & 0 \\ 0 & \frac{4\Delta t^2}{3} & 0 & \frac{4\Delta t}{2} & 0 \\ \frac{\pi}{9} \frac{\Delta t}{2} & 0 & \frac{\pi}{9} & 0 & 0 \\ 0 & \frac{4\Delta t}{2} & 0 & 4 & 0 \\ 0 & 0 & 0 & 0 & \frac{\pi}{18} \frac{(\Delta t)^2}{3} \end{bmatrix}.$$

For the process noise, the maximum change in β_k and α_k is considered, which is $\dot{\beta}_k < 2\text{m/s}$ and $\dot{\alpha}_k < 2(\max\{u_k\}) = \frac{\pi}{9}\text{rad/s}$, respectively. For $\hat{\theta}_k$, the same noise as α_k is considered. For our case, this resulted in a filter that was too conservative, so we multiplied our process noise matrix by a factor of 5×10^{-6} . The consistency results are discussed later in this section. Sensor measurements occur every 0.5s. The values for R are inspired by the noise in measurement of the bearing and range using a camera, as discussed earlier.

5.2 Estimation for Constant Velocity Targets

We assume that the UAV receives noisy measurements of the relative bearing and range from the target. An EKF is used to estimate the relative bearing, range, and their derivatives. Our EKF states are

$$\hat{q}_k = \begin{bmatrix} \hat{\alpha}_k \\ \hat{\beta}_k \\ \dot{\hat{\alpha}}_k \\ \dot{\hat{\beta}}_k \\ \hat{\theta}_k \end{bmatrix},$$

where $(\hat{\cdot})$ indicates an estimated value. Note that the change of heading of the UAV is the control command $u_k = \dot{\theta}_k$, and is assumed to be known.

The prediction equations for our states are

$$\begin{aligned}
\hat{\alpha}_k &= \hat{\alpha}_k^- + \dot{\hat{\alpha}}_k^- \Delta t, \\
\hat{\beta}_k &= \hat{\beta}_k^- + \dot{\hat{\beta}}_k^- \Delta t, \\
\dot{\hat{\alpha}}_k &= (\hat{\beta}_k^-)^{-1} (\hat{v}_{y_k}^- \cos(\hat{\alpha}_k^- + \hat{\theta}_k^-) \\
&\quad - \hat{v}_{x_k}^- \sin(\hat{\alpha}_k^- + \hat{\theta}_k^-) + \sin(\hat{\alpha}_k^-)) - u_k^-, \\
\dot{\hat{\beta}}_k &= \hat{v}_{x_k}^- \cos(\hat{\alpha}_k^- + \hat{\theta}_k^-) \\
&\quad + \hat{v}_{y_k}^- \sin(\hat{\alpha}_k^- + \hat{\theta}_k^-) - \cos(\hat{\alpha}_k^-) \\
\hat{\theta}_k &= \hat{\theta}_k^- + u_k \Delta t,
\end{aligned}$$

where $(\cdot)^-$ denotes the variable at the previous time step. Estimated values of the target velocity, \hat{v}_x and \hat{v}_y are calculated from the geometry of the UAV and the target as

$$\begin{aligned}
\hat{v}_x &= \hat{\beta}_k \cos(\hat{\alpha}_k + \hat{\theta}_k) - \hat{\beta}_k \sin(\hat{\alpha}_k + \hat{\theta}_k) (\dot{\hat{\alpha}}_k + \dot{\hat{\theta}}_k) + \cos(\hat{\theta}_k) \\
\hat{v}_y &= \hat{\beta}_k \sin(\hat{\alpha}_k + \hat{\theta}_k) + \hat{\beta}_k \cos(\hat{\alpha}_k + \hat{\theta}_k) (\dot{\hat{\alpha}}_k + \dot{\hat{\theta}}_k) + \sin(\hat{\theta}_k).
\end{aligned}$$

The error covariance P_k updates as

$$P_k = F_{q_k} P_k^- F_{q_k}^\top + Q.$$

The Jacobian matrix F_{q_k} for the k^{th} UAV with states \hat{q}_k is

$$F_{q_k} = \begin{bmatrix} 1 & 0 & \Delta t & 0 & 0 \\ 0 & 1 & 0 & \Delta t & 0 \\ \frac{\partial \dot{\hat{\alpha}}_k}{\partial \hat{\alpha}_k} & \frac{\partial \dot{\hat{\alpha}}_k}{\partial \hat{\beta}_k} & 1 & \frac{\partial \dot{\hat{\alpha}}_k}{\partial \hat{\beta}_k} & \frac{\partial \dot{\hat{\alpha}}_k}{\partial \hat{\theta}_k} \\ \frac{\partial \dot{\hat{\beta}}_k}{\partial \hat{\alpha}_k} & \frac{\partial \dot{\hat{\beta}}_k}{\partial \hat{\beta}_k} & \frac{\partial \dot{\hat{\beta}}_k}{\partial \hat{\alpha}_k} & 1 & \frac{\partial \dot{\hat{\beta}}_k}{\partial \hat{\theta}_k} \\ 0 & 0 & 0 & 0 & 1 \end{bmatrix},$$

where

$$\begin{aligned}
\frac{\partial \dot{\hat{\alpha}}_k}{\partial \hat{\alpha}_k} &= \frac{-\hat{v}_{y_k}^- \sin(\hat{\alpha}_k^- + \hat{\theta}_k^-) - \hat{v}_{x_k}^- \cos(\hat{\alpha}_k^- + \hat{\theta}_k^-) - \frac{\partial \hat{v}_{y_k}^-}{\partial \hat{\alpha}_k} \sin(\hat{\alpha}_k^- + \hat{\theta}_k^-) + \frac{\partial \hat{v}_{y_k}^-}{\partial \hat{\alpha}_k} \cos(\hat{\alpha}_k^- + \hat{\theta}_k^-) + \cos(\hat{\alpha}_k^-)}{\hat{\beta}_k^-} \\
\frac{\partial \dot{\hat{\alpha}}_k}{\partial \hat{\beta}_k} &= \frac{-\frac{\partial \hat{v}_{x_k}^-}{\partial \hat{\beta}_k} \sin(\hat{\alpha}_k^- + \hat{\theta}_k^-) + \frac{\partial \hat{v}_{y_k}^-}{\partial \hat{\beta}_k} \sin(\hat{\alpha}_k^- + \hat{\theta}_k^-) - \dot{\hat{\alpha}}_k - u_k^-}{\hat{\beta}_k^-} \\
\frac{\partial \dot{\hat{\alpha}}_k}{\partial \hat{\theta}_k} &= \frac{-\frac{\partial \hat{v}_{x_k}^-}{\partial \hat{\theta}_k} \sin(\hat{\alpha}_k^- + \hat{\theta}_k^-) + \frac{\partial \hat{v}_{y_k}^-}{\partial \hat{\theta}_k} \cos(\hat{\alpha}_k^- + \hat{\theta}_k^-)}{\hat{\beta}_k^-} \\
\frac{\partial \dot{\hat{\beta}}_k}{\partial \hat{\alpha}_k} &= \frac{-\hat{v}_{y_k}^- \sin(\hat{\alpha}_k^- + \hat{\theta}_k^-) - \hat{v}_{x_k}^- \cos(\hat{\alpha}_k^- + \hat{\theta}_k^-) - \frac{\partial \hat{v}_{x_k}^-}{\partial \hat{\alpha}_k} \sin(\hat{\alpha}_k^- + \hat{\theta}_k^-) + \frac{\partial \hat{v}_{y_k}^-}{\partial \hat{\alpha}_k} \cos(\hat{\alpha}_k^- + \hat{\theta}_k^-)}{\hat{\theta}_k^-} \\
\frac{\partial \dot{\hat{\beta}}_k}{\partial \hat{\beta}_k} &= -\hat{v}_{x_k}^- \sin(\hat{\alpha}_k^- + \hat{\theta}_k^-) + \hat{v}_{y_k}^- \cos(\hat{\alpha}_k^- + \hat{\theta}_k^-) + \frac{\partial \hat{v}_{x_k}^-}{\partial \hat{\beta}_k} \cos(\hat{\alpha}_k^- + \hat{\theta}_k^-) + \frac{\partial \hat{v}_{y_k}^-}{\partial \hat{\beta}_k} \sin(\hat{\alpha}_k^- + \hat{\theta}_k^-) + \sin(\hat{\alpha}_k^-) \\
\frac{\partial \dot{\hat{\beta}}_k}{\partial \hat{\alpha}_k} &= \frac{\partial \hat{v}_{x_k}^-}{\partial \hat{\alpha}_k} \cos(\hat{\alpha}_k^- + \hat{\theta}_k^-) + \frac{\partial \hat{v}_{y_k}^-}{\partial \hat{\alpha}_k} \sin(\hat{\alpha}_k^- + \hat{\theta}_k^-) \\
\frac{\partial \dot{\hat{\beta}}_k}{\partial \hat{\theta}_k} &= \frac{\partial \hat{v}_{x_k}^-}{\partial \hat{\theta}_k} \cos(\hat{\alpha}_k^- + \hat{\theta}_k^-) + \frac{\partial \hat{v}_{y_k}^-}{\partial \hat{\theta}_k} \sin(\hat{\alpha}_k^- + \hat{\theta}_k^-) \\
\frac{\partial \dot{\hat{\theta}}_k}{\partial \hat{\alpha}_k} &= -\hat{v}_{x_k}^- \sin(\hat{\alpha}_k^- + \hat{\theta}_k^-) + \hat{v}_{y_k}^- \cos(\hat{\alpha}_k^- + \hat{\theta}_k^-) + \frac{\partial \hat{v}_{x_k}^-}{\partial \hat{\alpha}_k} \cos(\hat{\alpha}_k^- + \hat{\theta}_k^-) + \frac{\partial \hat{v}_{y_k}^-}{\partial \hat{\alpha}_k} \sin(\hat{\alpha}_k^- + \hat{\theta}_k^-).
\end{aligned}$$

Only α_k and β_k are measured which implies the observation matrix is

$$H = \begin{bmatrix} 1 & 0 & 0 & 0 & 0 \\ 0 & 1 & 0 & 0 & 0 \end{bmatrix}.$$

Using the estimated values, the controller for stationary targets in Equation (3.12) becomes

$$u_k = \omega_0(1 - \hat{\beta}_k \cos(\hat{\alpha}_k)). \quad (5.1)$$

For constant velocity targets, the controllers from Equations (3.17) and (3.23) become

$$u_k = \frac{\hat{\beta}_k(f_{1k}^2(\hat{q}_k)) - K_1(\hat{\beta}_k - \omega_0^{-1}) - K_2(\hat{\beta}_k)}{\sin(\hat{\alpha}_k)} \quad (5.2)$$

and

$$u_k = \frac{\hat{\alpha}_{k_x}^2 + \hat{\alpha}_{k_y}^2}{\hat{\alpha}_{k_y}} \left(\frac{\hat{A}_k}{\hat{\alpha}_k} + \frac{(\hat{\alpha}_k - \omega_0^{-1})\hat{\beta}_k}{\hat{\alpha}_k - \hat{\alpha}_{k_d}} + K_1(\hat{\beta}_k - \omega_0^{-1})^2(\hat{\alpha}_k - \hat{\alpha}_{k_d}) + K_2(\hat{\alpha}_k - \hat{\alpha}_{k_d}) \right). \quad (5.3)$$

For constantly accelerating targets, the controllers in Equation (3.25) and (3.27) become

$$u_k = \frac{\hat{\beta}_k(f_{1k}^2(\hat{q}_k) + a_{x_k} \cos(\hat{\alpha}_k + \hat{\theta}_k) + a_{y_k} \sin(\hat{\alpha}_k + \hat{\theta}_k)) - K_1(\hat{\beta}_k - \omega_0^{-1}) - K_2(\hat{\beta}_k)}{\sin(\hat{\alpha}_k)} \quad (5.4)$$

and

$$u_k = \frac{\hat{\alpha}_{k_x}^2 + \hat{\alpha}_{k_y}^2}{\hat{\alpha}_{k_y}} \left(\frac{\hat{A}_k}{\hat{\beta}_k} + \frac{(\hat{\beta}_k - \omega_0^{-1})\hat{\beta}_k}{\hat{\alpha}_k - \hat{\alpha}_{k_d}} + K_1(\hat{\beta}_k - \omega_0^{-1})^2(\hat{\alpha}_k - \hat{\alpha}_{k_d}) + K_2(\hat{\alpha}_k - \hat{\alpha}_{k_d}) \right) + \frac{\alpha_{k_x}(a_{x_k} \cos(\hat{\theta}_k) + a_{y_k} \sin(\hat{\theta}_k)) + \alpha_{k_y}(a_{y_k} \cos(\hat{\theta}_k) - a_{x_k} \sin(\hat{\theta}_k))}{\alpha_{k_y}}. \quad (5.5)$$

In Equations (5.4) and (5.5), a_x and a_y are the known true accelerations. These values are not estimated as the errors in estimating the acceleration are too high for unit speed simulations and the proposed errors, and will be addressed in future work with UAVs flying at higher speeds.

The parameters from Equations (3.22), (3.19) and (3.21), \hat{A}_k , $\hat{\alpha}_{k_d}$ and $\hat{\alpha}_{k_d}$, are evaluated at estimated values $\hat{\alpha}_k$, $\hat{\beta}_k$ and $\hat{\theta}_k$. The controllers thus use estimated values of bearing $\hat{\alpha}_k$ and range $\hat{\beta}_k$ to calculate the desired change in heading u_k of the UAV_{*k*} at every time step.

In Chapter 6 simulations are shown that use controllers from Equations (5.1)-(5.4) to show the UAVs converge to circular trajectories using estimated values.

CHAPTER 6. SIMULATIONS AND RESULTS

In this chapter, results are presented for the encirclement of stationary and moving targets. We run simulations with different random initial positions of three UAVs encircling a target.

The parameters for all the simulations are the same, with the starting positions of the three UAVs defined randomly in an area of $60 \times 60 \text{m}^2$ and the headings, relative to a global frame, defined randomly in the range $[-\pi, \pi]$ radians. The estimated values of bearing $\hat{\alpha}_k$ and range $\hat{\beta}_k$ are also initialized randomly in ranges of $[-\pi, \pi]$ radians and $[-60, 60]$ m respectively. We run the simulations for 10,000s, with a timestep $\Delta t = 0.01$ s for the stationary target. For the constant velocity and accelerating targets, we run the simulations for 1,000s and 1,400s, respectively, with the same timestep, $\Delta t = 0.01$ s. We define the angular speed of the UAV as $\omega_0 = \frac{1}{30}$ radians/s which gives a radius of $\omega_0^{-1} = 30$ m. We also saturate the UAVs turn-rate to mimic a constraint on its bank angle. In [43], the authors describe a maximum bank angle of 69.1° for a fixed-wing. We use a more conservative approach and put a limit of $10^\circ/\text{s}$ on the turn rate, considering a coordinated turn with a maximum bank angle of 45° . This puts a saturation constraint on control u_k , with $u_{max} = \frac{\pi}{18}$ in Equation (2.2). Each experiment is seeded with the same starting conditions so that the results of the different controllers may be compared.

In the results for constant velocity and accelerating targets, we estimate all the variables, including range β_k , bearing α_k and their derivatives, as well as the local heading θ_k and the velocity of the target $v_{x_k} + iv_{y_k}$. For the accelerating targets, the acceleration $a_{x_k} + ia_{y_k}$ used in the controller Equation (3.27) is assumed to be known for the control, since we are not estimating acceleration of the target in Chapter 5.

6.1 Stationary Targets

Figure 6.1 shows a target encirclement simulation using the Lyapunov controller presented in Section 3.1 and revised with estimated parameters as in Equation (5.1). In this figure, the target

location is shown as a blue plus sign in the center of the frame. The random starting positions of each UAV are given by the three pink plus signs and each UAV trajectory is shown by a colored dashed line. As can be seen, regardless of their starting positions, all UAVs converge to a circular formation with a desired radius around the target.

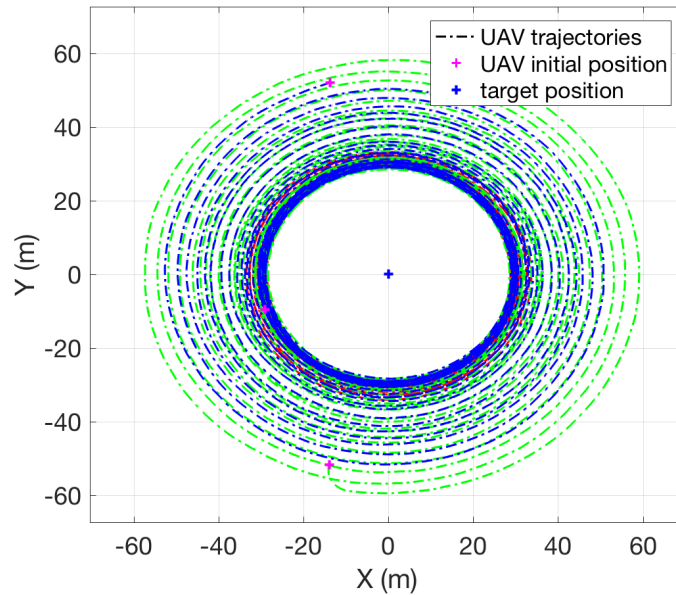


Figure 6.1: Trajectory of UAV encircling a stationary target for simulation time $t = [0,10000]$ s.

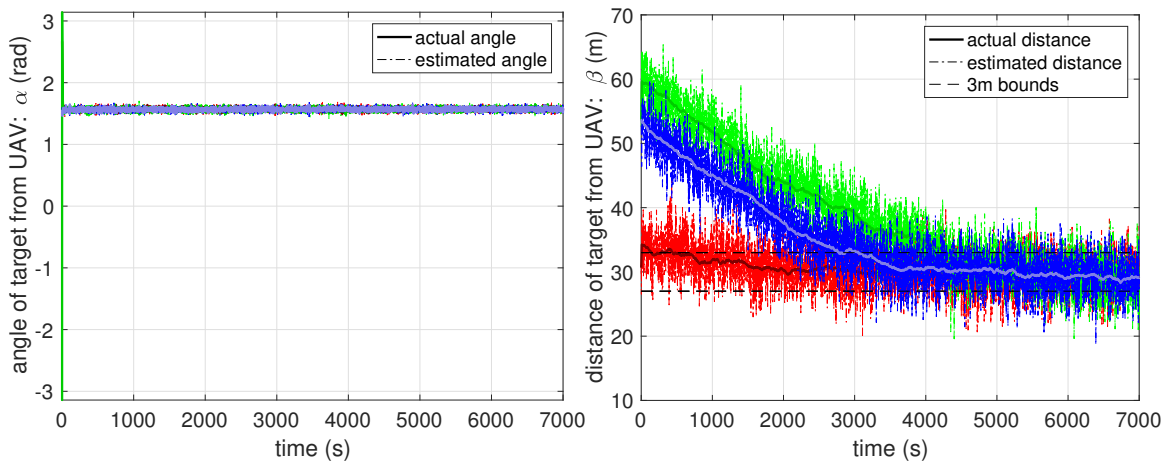


Figure 6.2: Bearing α_k (left) and range β_k (right) of the target with respect to the UAVs as a function of time for a stationary target.

Figure 6.2 (left) shows that α_k , the angle of the target with respect to the UAV, is constant for all UAVs at $\frac{\pi}{2}$ radians. The UAVs converge to the 30m radius circle, as seen in Figure 6.2 (right). The error in achieving the desired radius is $< 3\text{m}$, due to noisy measurements. The solid lines show the actual range/bearing of the target from the UAV, and the dashed lines show the estimated values from the EKF. The black dashed lines show the 3m bounds from the desired radius.

6.2 Constant Velocity Moving Targets

In the following simulations, the target moves at a constant velocity $v_{x_k} = 0.4\text{m/s}$ and $v_{y_k} = -0.1\text{m/s}$ in an inertial frame. The gains for the estimated moving controller in Equation (5.2) are set to $K_1 = 0.01$ and $K_2 = 0.05$. These gains are chosen by looking at the relative scale of the feedback linearized controller terms and the states, and then tuning for desired performance.

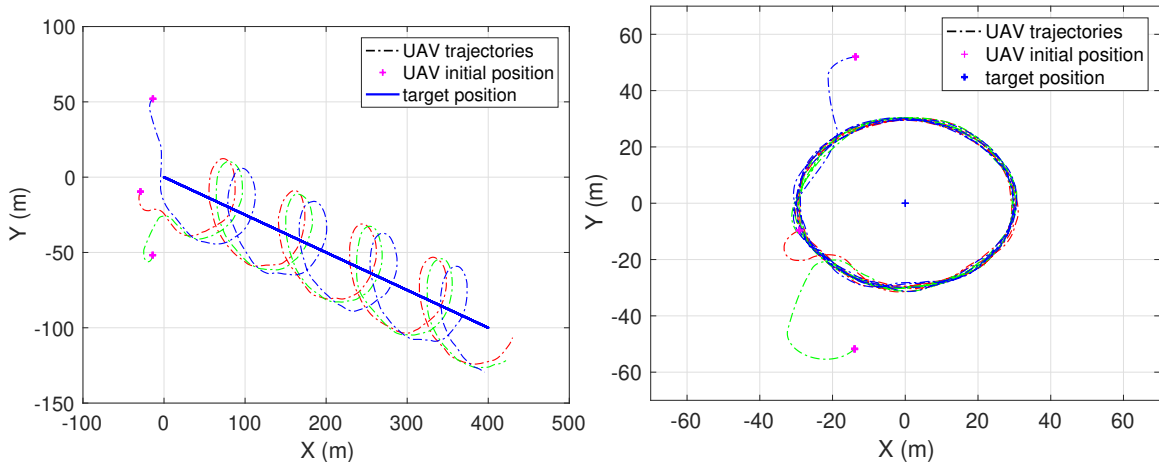


Figure 6.3: Trajectory of UAVs encircling a target moving with constant velocity $v_x + iv_y = (0.4 - i0.1)\text{m/s}$ for simulation time $t = [1, 1000]\text{s}$ in the inertial frame (left) and target moving frame (right).

Figure 6.3 (left) shows the encirclement of moving targets using the estimated moving controller. The blue line shows the true target position, with the dashed lines being the trajectories of the UAVs in an inertial frame while encircling the target. Figure 6.3 (right) shows the UAV's trajectories in a moving body frame centered at the target's location.

We can see from Figure 6.4 (left) that the bearing from the target for each UAV oscillates around $\pm \frac{\pi}{2}$ radians. The oscillations in the bearing are necessary for the UAV to compensate for the target motion (Equation (3.10)) and maintain a constant radius.

Figure 6.4 (right) illustrates that the distance of the target from the UAV converges to the desired radius $\omega_0^{-1} = 30\text{m}$. Also shown in this figure is the difference between the estimated range (dashed colored lines) and true range (solid colored lines). The UAV estimates converge to the true range values as the UAV encircles the target while mostly staying within 3m of the desired radius, marked by the black dashed lines.

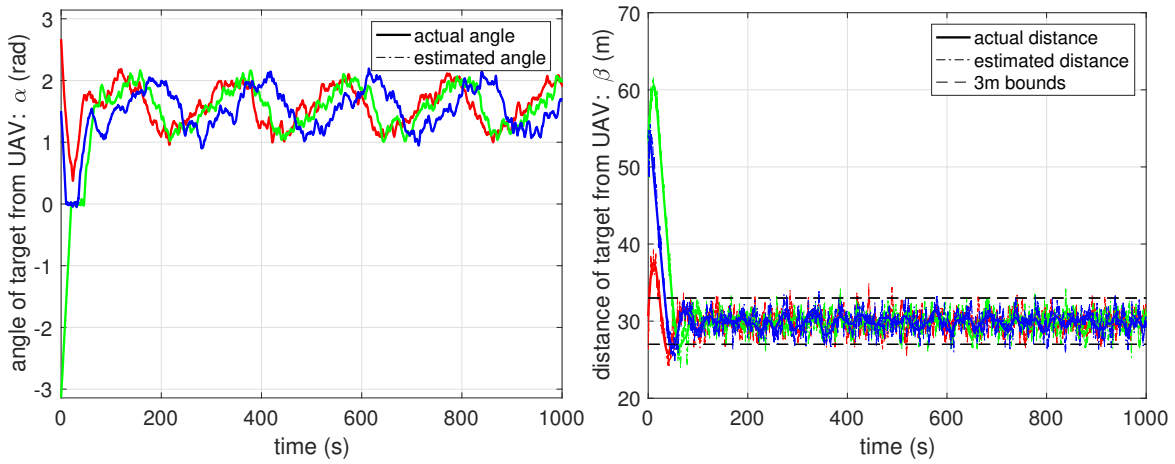


Figure 6.4: Bearing α_k (left) and range β_k (right) to the target with respect to the UAV as a function of time for a moving target with velocity $v_x + iv_y = (0.4 - i0.1)\text{m/s}$.

6.3 Directional Control with Constant Velocity Targets

We show results for the controller in Equation (3.23) proposed in Section 3.3. In Figure 6.5, we see that the UAVs start at random positions and headings, but always converge to a given direction. In the following results, the direction is clockwise for $d = -1$. The gains can be used to weight the convergence to the desired radius and bearing as defined in Equation (3.20), and are set to $K_1 = 0.1$ and $K_2 = 10$. These correspond to the scale of the error in α_k and β_k . Figure 6.6 shows that the bearing oscillates around $-\frac{\pi}{2}$ (left), and the distance from the target converges to 30m (right).

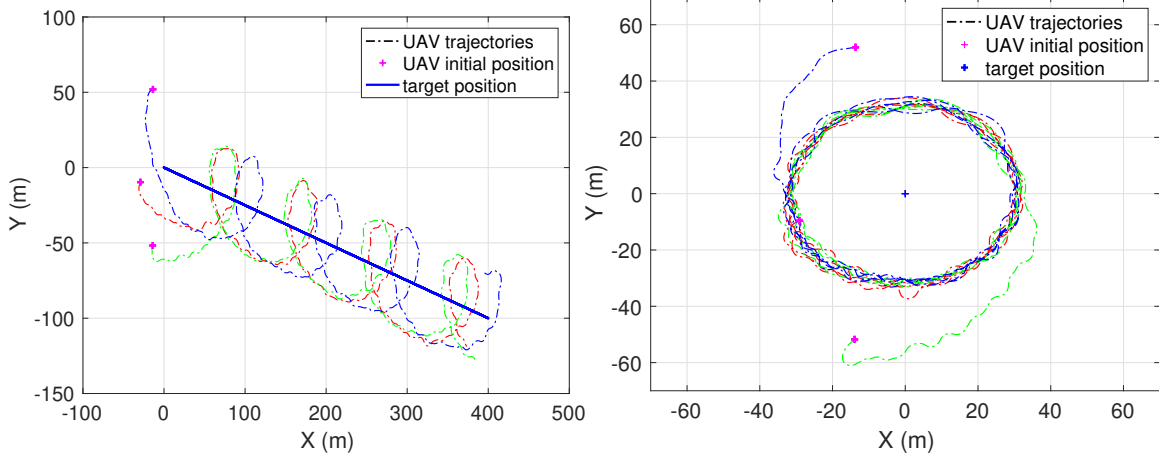


Figure 6.5: Constant velocity target encirclement with direction control in an inertial (left) and target moving frame (right) with velocity $v_x + iv_y = (0.4 - i0.1)m/s$.

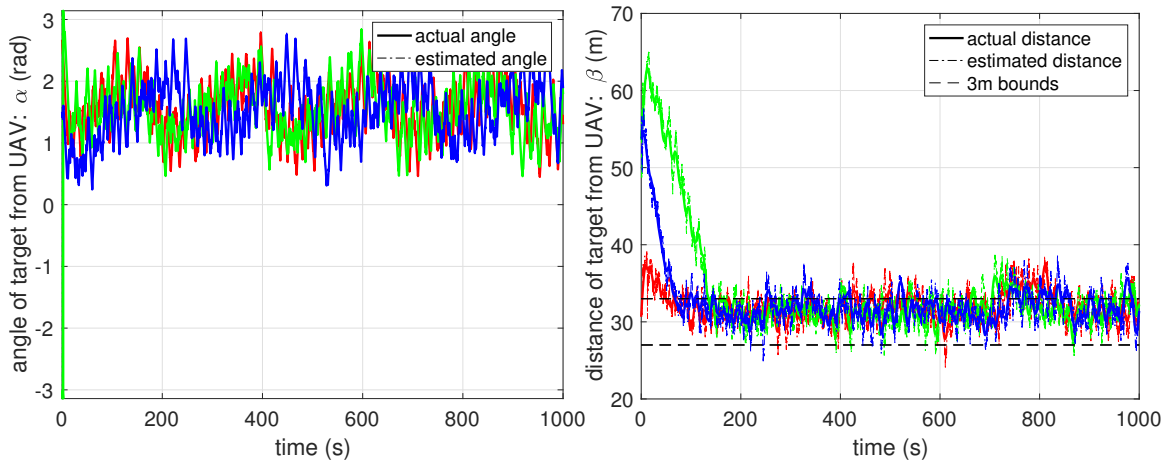


Figure 6.6: Bearing (left) and range (right) from target for a constant velocity target encirclement with direction control with velocity $v_x + iv_y = (0.4 - i0.1)m/s$.

6.4 Consistency of the Filter and Target Velocity Estimates for Constant Velocity Targets

We also validate the consistency of the filter by verifying that the values of the true range and bearing (β_k and α_k) lie within 2σ bounds of the estimated values 95% of the time. We show the consistency of a single simulation in Figure 6.7. Running 200 simulations for 1000s each, for a constant velocity target with the controller in Equation (5.2), we find that the range β_k lies within the bounds 96.54% of the time, and the bearing α_k lies within the bounds 94.80% of the time. This shows that the filter is close to consistent, since approximately 95% values lie within the 2σ

bounds when estimating the range and bearing while tracking the target, and the noise we are using is Gaussian.

For the 200 Monte Carlo simulations, we also calculate the error between the estimated and true values of bearing and range, and find that the error has a mean of 0 radians and 0.85m, and standard deviation of approximately $\frac{\pi}{120}$ radians and 2m, respectively. This depicts that the range estimates are slightly biased, accounting for the bias visible in Figure 6.4.

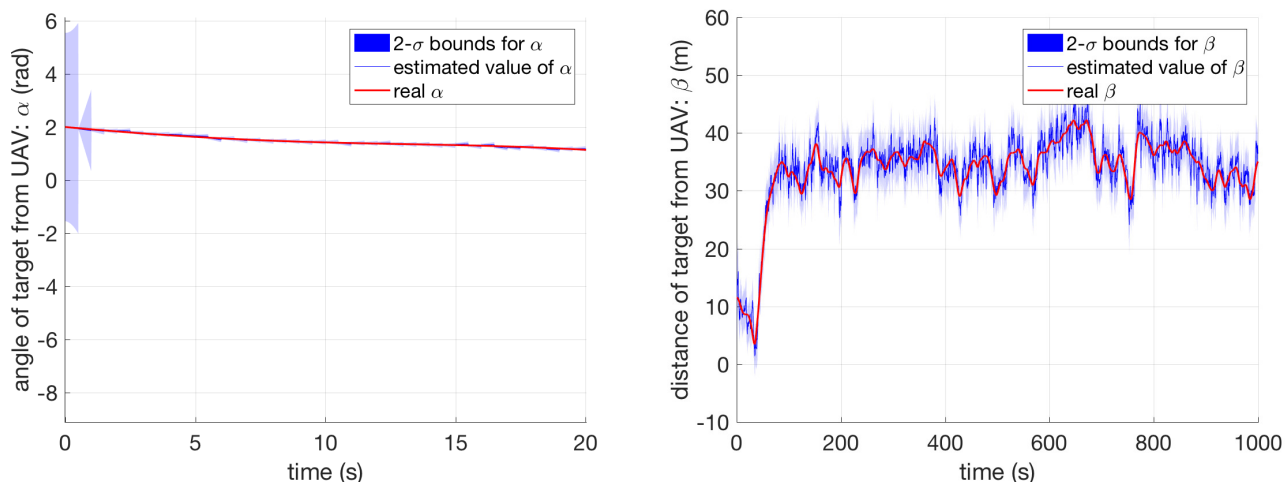


Figure 6.7: Consistency test for bearing (left) and range (right) for a random UAV. The red solid line shows the real bearing α_k . The shaded region shows the 2σ covariance bounds from the estimate shown with the blue solid line. The left figure shows the first 20s window to better see the real α_k enclosed by the bounds.

We can also see that the velocity estimates in Figure 6.8, corresponding to the controller from Equation (5.2) are noisy, but the controller still handles them well and converges to the loiter circle.

6.5 Constantly Accelerating Targets

We show results for the controller in Equation (3.25) proposed in Section 3.4. We see that the UAVs in Figure 6.9 start at random positions and headings, and converge to a circle around the accelerating target. Two UAVs converge clockwise, and one UAV converges to the counter-clockwise direction. The gains are set to $K_1 = 0.01$ and $K_2 = 0.05$. Figure 6.10 shows that the

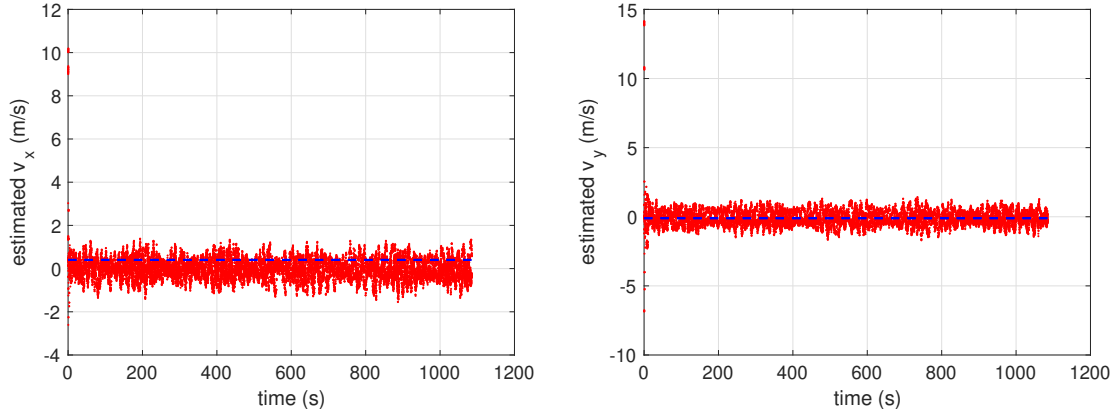


Figure 6.8: Estimated velocities (left: \hat{v}_x , right: \hat{v}_y) in an inertial frame, for a constant velocity target. The estimates have about 10 times the noise levels of the magnitude of the actual target velocities. The dashed blue line is the true value of the velocities in the inertial frame.

bearing oscillates around $\frac{\pi}{2}$ and $-\frac{\pi}{2}$ (left), and the distance from the target converges roughly to 30m (right).

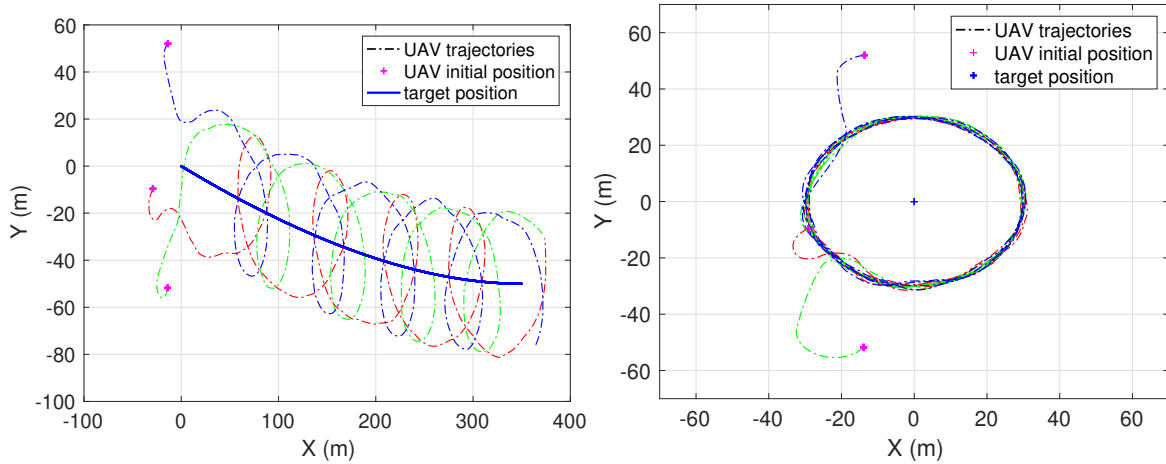


Figure 6.9: Constantly accelerating target encirclement in an inertial (left) and target moving frame (right) with initial velocity $v_x + iv_y = (0.4 - i0.1)m/s$ and acceleration $a_x + ia_y = (-0.0001 + i0.0001)m/s^2$.

6.6 Constantly Accelerating Targets with Direction Control

We show results for the controller in Equation (3.27) proposed in Section 3.5. We see that the UAVs in Figure 6.11 start at random positions and headings, and converge to a circle around the

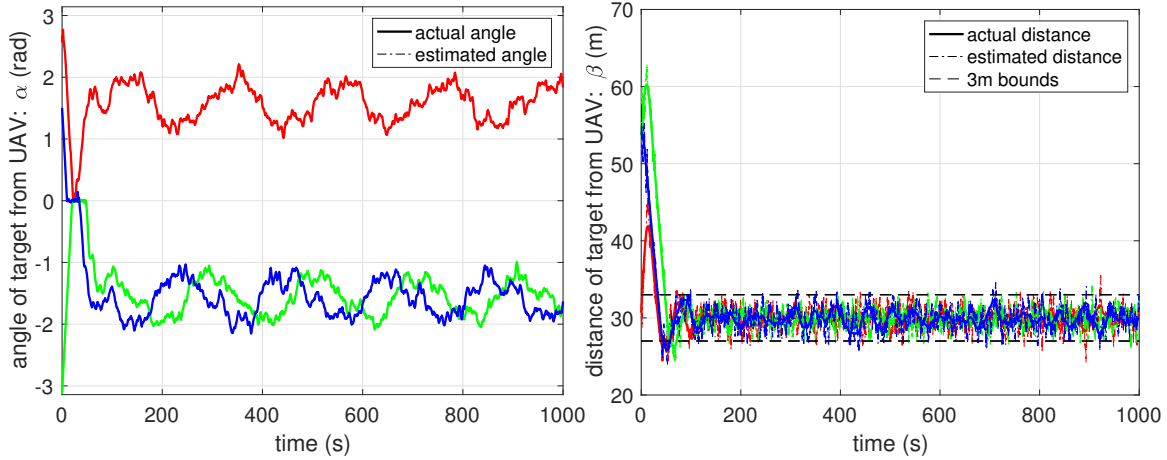


Figure 6.10: Bearing (left) and range (right) from a constantly accelerating target with initial velocity $v_x + iv_y = (0.4 - i0.1)m/s$ and acceleration $a_x + ia_y = (-0.0001 + i0.0001)m/s^2$.

accelerating target in one direction. The gains are set to $K_1 = 0.1$ and $K_2 = 10$. Figure 6.12 shows that the bearing oscillates around $-\frac{\pi}{2}$ (left), and the distance from the target converges roughly to 30m (right).

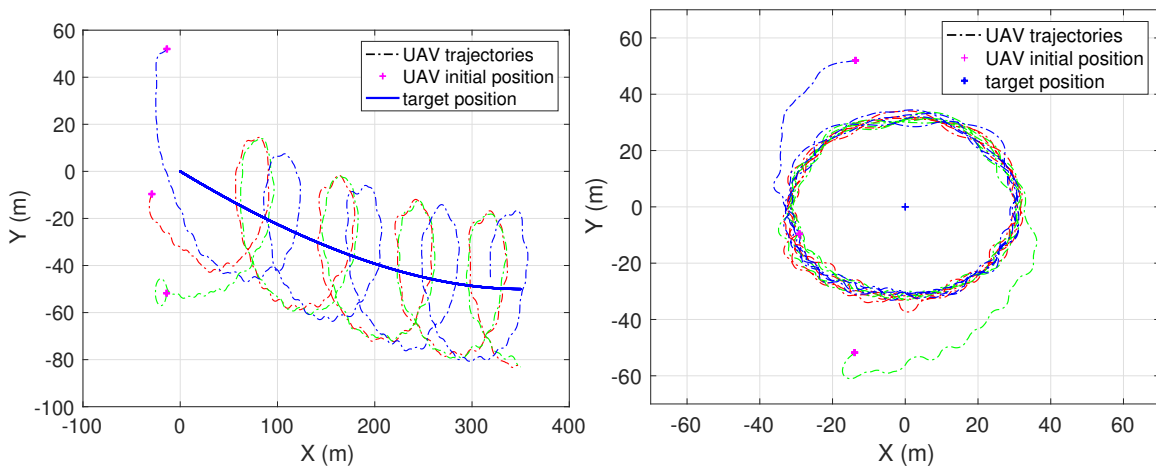


Figure 6.11: Constantly accelerating target encirclement with direction control in an inertial (left) and target moving frame (right) with initial velocity $v_x + iv_y = (0.4 - i0.1)m/s$ and acceleration $a_x + ia_y = (-0.0001 + i0.0001)m/s^2$.

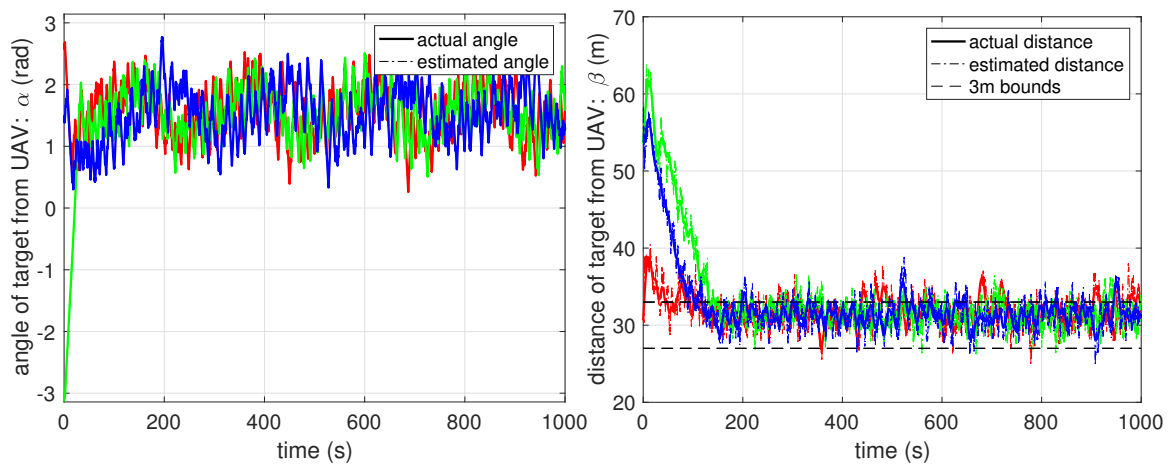


Figure 6.12: Bearing (left) and range (right) from a constantly accelerating target with direction control. The initial velocity is $v_x + iv_y = (0.4 - i0.1)m/s$ and acceleration is $a_x + ia_y = (-0.0001 + i0.0001)m/s^2$.

CHAPTER 7. CONCLUSION

This work designs controllers for target encirclement using relative information of range and bearing from the target, and knowledge of the local heading of the UAV. Each UAV starts in its own frame of reference and then converges to a loiter circle around a target. We also present a framework to estimate and filter these measurements along with the velocity of the UAV, and use these in the controller. Simulation results show that the controller is able to work well with noise levels inspired from literature involving real field tests.

7.1 Control Strategies

We present a controller that encircles stationary targets, using only range and bearing measurements from the target. We show that the control will stabilize all UAVs to the circular formation with a constant radius. We also propose a feedback linearized controller to encircle targets moving with a constant velocity and show that the constant radius circle is stable. In both cases, we show convergence to a fixed radius circle with numerical simulations using noisy measurements of range and bearing. We show that we can control the direction of encirclement as well.

We show encirclement of a constantly accelerating target, with known acceleration using a feedback linearized controller and Lyapunov's direct method for controlling the direction of encirclement of accelerating targets. We also show proofs of stability for both these controllers.

Future work would include overcoming the challenge of estimating the small acceleration values. We also want to be able to use only relative measurements of range and bearing to drive the UAVs in circles around the constantly accelerating targets while estimating the target motion. Currently the velocity estimates also have a high amount of noise, about ten times the actual target velocities, due to the error margins we consider inspired from literature with real-world experiments, and our assumption only considering unit UAV speed. In the future, we would extend the controllers to incorporate a constant, higher UAV velocity, which will be more realistic with the

noise used in range and bearing, and thus give us better estimates. This will also enable us to test the controller in more realistic situations, for flight tests and high-fidelity simulations.

7.2 Multi-Agent Coordination

We extend the constant velocity controller to arrange the UAVs in symmetric formations around the circle, focusing on an equal temporal spacing. These formations, called time-splay [29] allow us to have a better coverage around the target at all time. This would be useful in cases of UAV injection or attrition. Here the time-splay formation would reduce the time to re-arrange the UAVs around the target. Future work will include discussion and inclusion of a deeper analysis of region of attraction for each symmetric formation. We also discuss how inter-group communication is feasible and can be used for spreading information in cases where groups are too far for direct communication. In this case, we assume knowledge of group locations. In our analysis, we see that after a certain frequency of travel times, the time taken for the information to dissipate plateaus. Future work would include exploring the extension of this to estimated group positions to enable group communication in the relative information only scenario. We also aim to study the scenarios where the information is noisy, and multiple groups have different information, and incorporate a "rest" period for the UAVs who joined a new group. Future work would also include studying group leaving patterns for UAVs to maintain roughly equal number of UAVs on all targets, thus dividing the work-load equally.

Since we are estimating values of the local heading, range and bearing to the target, communication between UAVs could be used to improve the estimates, assuming there is some information that the UAVs have in common. Future work will also include incorporating an observer to estimate each UAV's change in heading and eliminate the need for UAVs to know their orientation relative to a local frame. Additionally, we aim to incorporate measurements from peer UAVs, using only their relative range to improve each UAV's estimate of the target velocity. The scenario in Figure 7.1 is a proposed framework that is under work for sharing between two UAVs in communication range, where they are with respect to the target using only range between the UAVs and their noisy range and bearing from the target.

In our case, this communication protocol requires us to consider the moving target as the common frame, and the angle Z (refer Figure 7.1) is calculated as

$$Z = \text{sgn}(Z)(|\alpha_{k1} + \theta_{k1}| + |\alpha_{k1} + \theta_{k1}| - (\psi_1 - \psi_2)),$$

where sgn is defined as

$$\text{sgn}(Z) = \begin{cases} -1, & \text{sgn}(Z) < 0 \\ 0, & \text{sgn}(Z) = 0 \\ 1, & \text{sgn}(Z) > 0. \end{cases}$$

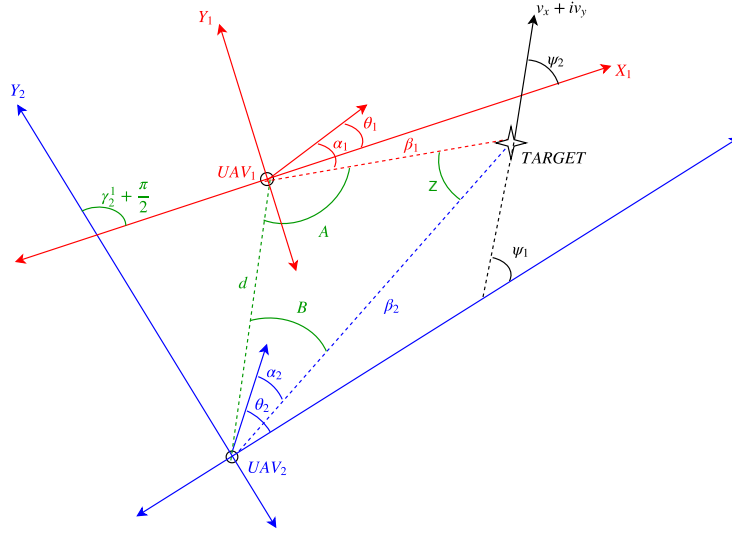


Figure 7.1: Communication setup for an example two UAVs

This setup may yields imaginary results (invalid input in inverse trigonometric functions), due to the noisy range and bearing of the system causing the UAV to have a false sense of where it is. We realize that this setup is un-suitable for high noise systems for sharing information between UAVs. We plan to further explore this to find a suitable method to share information with knowledge of just the range between the UAVs. Finding noise margins for our system for which information sharing is possible is our next step into multi-group decentralized target encirclement with formation control.

REFERENCES

- [1] R. Sepulchre, D. A. Paley, and N. E. Leonard, “Stabilization of planar collective motion with limited communication,” *IEEE Transactions on Automatic Control*, vol. 53, no. 3, pp. 706–719, 2008. vi, 27, 28, 30
- [2] D. Chabot and D. M. Bird, “Wildlife research and management methods in the 21st century: Where do unmanned aircraft fit in?” *Journal of Unmanned Vehicle Systems*, vol. 3, no. 4, pp. 137–155, 2015. [Online]. Available: <https://doi.org/10.1139/juvs-2015-0021> 1
- [3] J. Akagi, B. Moon, X. Chen, and C. Peterson, “Gesture commands for controlling high-level UAV behavior,” in *2019 International Conference on Unmanned Aircraft Systems (ICUAS’19)*. ICUAS, 2019. 1
- [4] M. A. Goodrich, B. S. Morse, D. Gerhardt, J. L. Cooper, M. Quigley, J. A. Adams, and C. Humphrey, “Supporting wilderness search and rescue using a camera-equipped mini UAV,” *Journal of Field Robotics*, vol. 25, no. 1-2, pp. 89–110, 2008. 1
- [5] V. N. Dobrokhodov, I. I. Kaminer, K. D. Jones, and R. Ghabcheloo, “Vision-based tracking and motion estimation for moving targets using small UAVs,” in *2006 American Control Conference*. IEEE, 2006, pp. 6–pp. 1
- [6] A. Sinha, T. Kirubarajan, and Y. Bar-Shalom, “Optimal cooperative placement of UAVs for ground target tracking with doppler radar,” in *Signal Processing, Sensor Fusion, and Target Recognition XIII*, vol. 5429. International Society for Optics and Photonics, 2004, pp. 95–104. 1
- [7] C. Chen and R. Stettner, “Drogue tracking using 3D flash LIDAR for autonomous aerial refueling,” in *Laser Radar Technology and Applications XVI*, vol. 8037. International Society for Optics and Photonics, 2011, p. 80370Q. 1
- [8] S. Ahrens, D. Levine, G. Andrews, and J. P. How, “Vision-based guidance and control of a hovering vehicle in unknown, GPS-denied environments,” in *2009 IEEE International Conference on Robotics and Automation*. IEEE, 2009, pp. 2643–2648. 1

- [9] R. A. Newcombe and A. J. Davison, “Live dense reconstruction with a single moving camera,” in *Computer Vision and Pattern Recognition (CVPR), 2010 IEEE Conference on*. IEEE, 2010, pp. 1498–1505. 2
- [10] C. Forster, M. Faessler, F. Fontana, M. Werlberger, and D. Scaramuzza, “Continuous on-board monocular-vision-based elevation mapping applied to autonomous landing of micro aerial vehicles,” in *2015 IEEE International Conference on Robotics and Automation (ICRA)*. IEEE, 2015, pp. 111–118. 2
- [11] J. Nielsen and R. W. Beard, “Ground target tracking using a monocular camera and IMU in a nonlinear observer SLAM framework,” *2018 Annual American Control Conference (ACC)*, pp. 6457–6462, 2018. 2
- [12] M. Pachter, N. Ceccarelli, and P. R. Chandler, “Vision-based target geo-location using camera equipped MAVs,” in *2007 46th IEEE Conference on Decision and Control*. IEEE, 2007, pp. 2333–2338. 2, 36
- [13] M. D. Warren, “Long-range stereo visual odometry for unmanned aerial vehicles,” Ph.D. dissertation, Queensland University of Technology, 2015. 2
- [14] S. Agarwal, S. B. Lazarus, and A. Savvaris, “Monocular vision based navigation and localisation in indoor environments,” *IFAC Proceedings Volumes*, vol. 45, no. 1, pp. 97–102, 2012. 2
- [15] M. Perrollaz, R. Labayrade, C. Royere, N. Hautiere, and D. Aubert, “Long range obstacle detection using laser scanner and stereovision,” in *2006 IEEE intelligent vehicles symposium*. IEEE, 2006, pp. 182–187. 2
- [16] X. Wang, J. Liu, and Q. Zhou, “Real-time multi-target localization from unmanned aerial vehicles,” *Sensors*, vol. 17, no. 1, p. 33, 2017. 2
- [17] M. Mostafa, S. Zahran, A. Moussa, N. El-Sheimy, and A. Sesay, “Radar and visual odometry integrated system aided navigation for UAVs in GNSS denied environment,” *Sensors*, vol. 18, no. 9, p. 2776, 2018. 2

- [18] M. Zhang and H. H. Liu, “Cooperative tracking a moving target using multiple fixed-wing UAVs,” *Journal of Intelligent & Robotic Systems*, vol. 81, no. 3-4, pp. 505–529, 2016. 2
- [19] E. W. Frew, D. A. Lawrence, C. Dixon, J. Elston, and W. J. Pisano, “Lyapunov guidance vector fields for unmanned aircraft applications,” in *American Control Conference, 2007. ACC’07.* IEEE, 2007, pp. 371–376. 2
- [20] Y. Cao, J. Muse, D. Casbeer, and D. Kingston, “Circumnavigation of an unknown target using UAVs with range and range rate measurements,” in *Decision and Control (CDC), 2013 IEEE 52nd Annual Conference on.* IEEE, 2013, pp. 3617–3622. 2
- [21] D. Milutinović, D. Casbeer, Y. Cao, and D. Kingston, “Coordinate frame free dubins vehicle circumnavigation using only range-based measurements,” *International Journal of Robust and Nonlinear Control*, vol. 27, no. 16, pp. 2937–2960, 2017. 2
- [22] A. S. Matveev, H. Teimoori, and A. V. Savkin, “The problem of target following based on range-only measurements for car-like robots,” in *Decision and Control, 2009 held jointly with the 2009 28th Chinese Control Conference. CDC/CCC 2009. Proceedings of the 48th IEEE Conference on.* IEEE, 2009, pp. 8537–8542. 2, 3, 4
- [23] M. Deghat, I. Shames, B. D. Anderson, and C. Yu, “Target localization and circumnavigation using bearing measurements in 2D,” in *Decision and Control (CDC), 2010 49th IEEE Conference on.* IEEE, 2010, pp. 334–339. 2
- [24] A. Hashemi, Y. Cao, D. W. Casbeer, and G. Yin, “Unmanned aerial vehicle circumnavigation using noisy range-based measurements without global positioning system information,” *Journal of Dynamic Systems, Measurement, and Control*, vol. 137, no. 3, pp. 031 003–031 003, 2015. 2
- [25] T. H. Summers, M. R. Akella, and M. J. Mears, “Coordinated standoff tracking of moving targets: Control laws and information architectures,” *Journal of Guidance, Control, and Dynamics*, vol. 32, no. 1, pp. 56–69, 2009. 2, 3, 4

- [26] H. Oh, S. Kim, A. Tsourdos, and B. A. White, “Decentralised standoff tracking of moving targets using adaptive sliding mode control for UAVs,” *Journal of Intelligent & Robotic Systems*, vol. 76, no. 1, pp. 169–183, 2014. 2
- [27] R. Wise and R. Rysdyk, “UAV coordination for autonomous target tracking,” in *AIAA Guidance, Navigation, and Control Conference and Exhibit*, 2006, p. 6453. 2
- [28] P. Theodorakopoulos and S. Lacroix, “A strategy for tracking a ground target with a UAV,” in *Intelligent Robots and Systems, 2008. IROS 2008. IEEE/RSJ International Conference on*. IEEE, 2008, pp. 1254–1259. 3
- [29] C. Peterson and D. A. Paley, “Multivehicle Coordination in an Estimated Time-Varying Flow-field,” *Journal of Guidance, Control, and Dynamics*, vol. 34, no. 1, pp. 177–191, 2011. 3, 4, 10, 26, 27, 29, 31, 51
- [30] H. Oh, S. Kim, H. Shin, and A. Tsourdos, “Coordinated standoff tracking of moving target groups using multiple UAVs,” *IEEE Transactions on Aerospace and Electronic Systems*, vol. 51, no. 2, pp. 1501–1514, 2015. 4
- [31] R. P. Anderson and D. Milutinović, “A stochastic approach to Dubins vehicle tracking problems,” *IEEE Transactions on Automatic Control*, vol. 59, no. 10, pp. 2801–2806, 2014. 4
- [32] D. A. Paley and C. Peterson, “Stabilization of collective motion in a time-invariant flowfield,” *Journal of Guidance, Control, and Dynamics*, vol. 32, no. 3, pp. 771–779, 2009. 4, 26, 27, 29
- [33] L. Sattenspiel and K. Dietz, “A structured epidemic model incorporating geographic mobility among regions,” *Mathematical Biosciences*, vol. 91, no. 1995, pp. 71–91, 1994. 4, 26, 31, 32
- [34] F. Bullo, R. Carli, and P. Frasca, “Gossip coverage control for robotic networks: Dynamical systems on the space of partitions,” *SIAM Journal on Control and Optimization*, vol. 50, no. 1, pp. 419–447, 2009. [Online]. Available: <http://arxiv.org/abs/0903.3642> 4, 26
- [35] M. Franceschelli, D. Rosa, C. Seatzu, and F. Bullo, “Gossip algorithms for heterogeneous multi-vehicle routing problems,” *Nonlinear Analysis: Hybrid Systems*, vol. 10, no. 1, pp. 156–174, 2013. [Online]. Available: <http://dx.doi.org/10.1016/j.nahs.2013.03.001> 4, 26, 31

- [36] G. R. Mallik, S. Daingade, and A. Sinha, "Consensus based deviated cyclic pursuit for target tracking applications," in *2015 European Control Conference (ECC)*. IEEE, 2015, pp. 1718–1723. 7
- [37] T. Lee, K. Song, C. Lee, and C. Teng, "Tracking control of unicycle-modeled mobile robots using a saturation feedback controller," *IEEE transactions on control systems technology*, vol. 9, no. 2, pp. 305–318, 2001. 7
- [38] L. Briñón-Arranz, A. Seuret, and A. Pascoal, "Target tracking via a circular formation of unicycles," *IFAC-PapersOnLine*, vol. 50, no. 1, pp. 5782–5787, 2017. 7
- [39] H. K. Khalil, *Nonlinear systems; 3rd ed.* Upper Saddle River, NJ: Prentice-Hall, 2002. [Online]. Available: <https://cds.cern.ch/record/1173048> 13, 15, 21, 25, 31
- [40] D. Kingston and R. W. Beard, "UAV splay state configuration for moving targets in wind," in *Advances in Cooperative Control and Optimization*. Springer, 2007, pp. 109–128. 26
- [41] R. A. Horn, "The Hadamard product," in *Proc. Symp. Appl. Math*, vol. 40, 1990, pp. 87–169. 30
- [42] Y. Bar-Shalom, X. R. Li, and T. Kirubarajan, *Estimation with applications to tracking and navigation: theory algorithms and software*. John Wiley & Sons, 2004. 37
- [43] J. N. Ostler, W. J. Bowman, D. O. Snyder, and T. W. McLain, "Performance flight testing of small, electric powered unmanned aerial vehicles," *International Journal of Micro Air Vehicles*, vol. 1, no. 3, pp. 155–171, 2009. 41

APPENDIX A. STATIONARY TARGET ENCIRCLEMENT WITH SPEED CONTROL

To generalize our control algorithms and incorporate them with real scenarios (high-fidelity simulations, hardware tests), we need to take into consideration the airspeed of the UAV. We present an example here for the stationary case, of how the airspeed s can be incorporated in the proposed control algorithms. The new dynamics become

$$\dot{r}_k = s e^{i\theta_k}. \quad (\text{A.1})$$

Equation (3.1) changes to

$$c_k = r_k + s\omega_0^{-1} i e^{i\theta_k}, \quad (\text{A.2})$$

where $s\omega_0$ is the radius of the circle. Thus our error dynamics, using the error from Equation (3.4) become

$$\dot{e} = -\dot{c}_k = -s e^{i\theta_k} + s\omega_0^{-1} e^{i\theta_k} \dot{\theta}_k. \quad (\text{A.3})$$

Our new controller is given by

$$u_k = \omega_0(1 - s\beta_k \cos(\alpha_k)). \quad (\text{A.4})$$

Figure A.1 shows a UAV converging to a loiter circle with radius $s\omega_0^{-1} = 30m$. Here $s = 5$ and $\omega_0^{-1} = 6$.

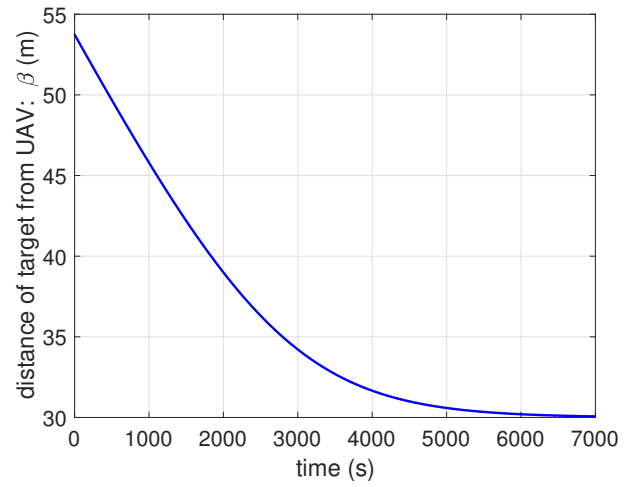
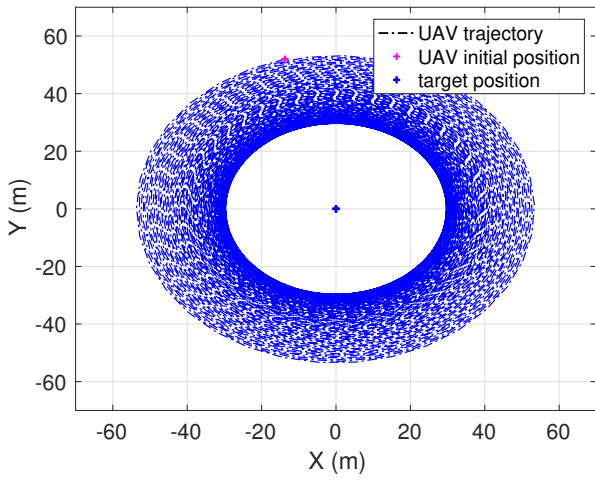


Figure A.1: (left) The UAV converges to the loiter circle. (right) The range converges to 30m.